Examination of varying mixed-phase stratocumulus clouds in terms of their properties, ice processes and aerosol-cloud interactions between polar and midlatitude cases: An attempt to propose a microphysical factor to explain the variation

Seoung Soo Lee[1,2,3], Chang-Hoon Jung[4], Jinho Choi[5], Young Jun Yoon[6], Junshik Um[5,7], Youtong Zheng[8], Jianping Guo[9], Manguttathil. G. Manoj[10], Sang-Keun Song[11]

[1]Science and Technology Corporation, Hampton, Virginia

[2]Earth System Science Interdisciplinary Center, University of Maryland, College Park, Maryland, USA

[3]Research Center for Climate Sciences, Pusan National University, Busan, Republic of Korea

[4]Department of Health Management, Kyungin Women's University, Incheon, Republic of Korea

[5]Department of Atmospheric Sciences, Pusan National University, Busan, Republic of Korea

[6]Korea Polar Research Institute, Incheon, Republic of Korea

[7]Institute of Environmental Studies, Pusan National University, Busan, Republic of Korea

[8]Department of Earth and Atmospheric Sciences, University of Houston, Houston, Texas, USA

[9]State Key Laboratory of Severe Weather, Chinese Academy of Meteorological Sciences, Beijing 100081, China

[10]Advanced Centre for Atmospheric Radar Research, Cochin University of Science and Technology, Kerala, India

[11]Department of Earth and Marine Sciences, Jeju National University, Jeju, Republic of Korea

Corresponding author: Seoung Soo Lee, Chang-Hoon Jung and Sang-Keun Song
Office: (303) 497-6615
Cell: (609) 375-6685
Fax: (303) 497-5318
E-mail: cumulss@gmail.com, slee1247@umd.edu

Abstract

This study examines the ratio of ice crystal number concentration (ICNC) to cloud droplet number concentration (CDNC), which is ICNC/CDNC, in mixed-phase stratocumulus clouds. This examination is performed using a large-eddy simulation (LES) framework and one of efforts toward a more general understanding of mechanisms controlling cloud development, aerosol-cloud interactions and impacts of ice processes on them in mixed-phase stratocumulus clouds. For the examination, this study compares a case of polar mixed-phase stratocumulus clouds to that of midlatitude mixed-phase stratocumulus clouds with weak precipitation. It is found that ICNC/CDNC plays a critical role in making differences in cloud development with respect to the relative proportion of liquid and ice mass between the cases by affecting in-cloud latent-heat processes. Note that this proportion has an important implication for cloud radiative properties and thus climate. It is also found that ICNC/CDNC plays a critical role in making differences in interactions between clouds and aerosols and impacts of ice processes on clouds and their interactions with aerosols between the cases by affecting in-cloud latent-heat processes. Findings of this study suggest that ICNC/CDNC can be a simplified general factor that contributes to a more general understanding and parameterizations of mixed-phase clouds, their interactions with aerosols and roles of ice processes in them.

1. Introduction

Stratiform clouds (e.g., stratus and stratocumulus clouds) have significant impacts on climate (Warren et al. 1986; Stephens and Greenwald 1991; Hartmann et al. 1992; Hahn and Warren 2007; Wood, 2012; Dione et al., 2019; Zheng et al., 2021). Since industrialization, aerosol concentrations have increased and this has had impacts on stratiform clouds and climate (Twomey, 1974; Albrecht, 1989; Ackerman et al., 2004). However, our level of understanding of these clouds and impacts has been low and this has caused the highest uncertainty in the prediction of future climate (Ramaswamy et al., 2001; Forster et al., 2007; Knippertz et al., 2011; Hannak et al., 2017). Stratiform clouds can be classified into warm and mixed-phase clouds. Mixed-phase stratiform clouds involve ice processes and frequently form in midlatitude and polar regions. When mixed-phase stratiform clouds are associated with convective clouds, they can form even in the tropical region. Most previous studies have focused on warm clouds and their interactions with aerosols, whereas the mixed-phase stratiform clouds and their interactions with aerosols are poorly understood mainly due to the more complex ice processes. Hence, mixed-phase stratiform clouds and their interactions with aerosols account for the uncertainty more than warm clouds and their interactions with aerosols (Ramaswamy et al., 2001; Forster et al., 2007; Wood, 2012; IPCC, 2021; Li et al., 2022).

The relative proportion of liquid mass, which can be represented by liquid-water content (LWC) or liquid-water path (LWP), and ice mass, which can be represented by ice-water content (IWC) or ice-water path (IWP), in mixed-phase stratiform clouds plays a critical role in cloud radiative properties and thus their climate feedbacks (Tsushima et al., 2006; Choi et al., 2010 and 2014; Gettelman et al., 2012; Zhang et al., 2019). The relative proportion is defined to be IWC (IWP) over LWC (LWP) or IWC/LWC (IWP/LWP) in this study. Motivated by this and the above-mentioned uncertainty, this study aims to improve our understanding of mixed-phase stratiform clouds and their interactions with aerosols with the emphasis on ice processes and IWC/LWC (or IWP/LWP).

Lee et al. (2021) have investigated mixed-phase stratocumulus clouds in a midlatitude region and found that microphysical latent-heat processes are more important in the development of mixed-phase stratiform clouds and their interactions with aerosols than entrainment and sedimentation processes. Lee et al. (2021) have found that a microphysical factor, the ratio of ice crystal number concentration (ICNC) to cloud droplet number concentration (CDNC) or ICNC/CDNC, play an important role in latent processes, the development of mixed-phase stratiform clouds and their interactions with aerosols. In particular, Lee et al. (2021) have found that IWC/LWC or IWP/LWP is strongly affected by ICNC/CDNC. This is because deposition and condensation of water vapor occur on the surface of ice crystals and droplets, respectively. Thus, ice crystals and droplets act as sources of deposition and condensation, respectively. Then, ice crystals and droplets act as sources of IWC (or IWP) and LWC (or LWP), respectively. More ice crystals and droplets provide the greater integrated surface area of ice crystals and droplets and induce more deposition and condensation, respectively, for a given environmental condition (Lee et al., 2009; Khain et al., 2012; Fan et al., 2018; Chua and Ming, 2020; Lee et al., 2021). The higher ICNC/CDNC means more ice crystals or sources of deposition per a droplet as a source of condensation in a given group of ice crystals and droplets. Thus, the higher ICNC/CDNC enables more deposition per unit condensation to occur, which can raise IWC/LWC or IWP/LWP.

Mixed-phase stratocumulus clouds in different regions are known to have different IWC/LWC or IWP/LWP and aerosol-cloud interactions (e.g., Choi et al., 2010 and 2014; Zhang et al., 2019). Lots of factors such as environmental conditions, which can be represented by variables such as temperature, humidity and wind shear, and macrophysical factors one of which is the relative locations of ice-crystal and droplet layers, can explain those differences. Choi et al. (2010 and 2014) and Zhang et al. (2019) have shown that as temperature lowers, IWC/LWC or IWP/LWP tends to increase and indicated that temperature is a primary environmental condition to explain the differences in IWC/LWC among different regions or clouds. However, Choi et al. (2010 and 2014) and Zhang et al. (2019) have not discussed process-level mechanisms that govern the role of temperature in those differences.

It is important to establish a general principle that explains the differences in LWC/LWC and aerosol-cloud interactions among regions, since the general principle is useful in the development of a more general or comprehensive parameterization of stratocumulus clouds and their interactions with aerosols for climate models. This contributes to the better prediction of future climate, considering that the absence of the comprehensive parameterization has been considered one of the biggest obstacles to the better prediction (Ramaswamy et al., 2001; Foster et al., 2007; Stevens and Feingold, 2009).

As a way of contributing to the establishment of the general principle, this study attempts to take ICNC/CDNC as a general factor, which can constitute the general principle, to explain the differences in IWC/LWC (or IWP/LWP) and aerosol-cloud interactions among clouds. This study also attempts to elucidate how ice processes differentiate mixed-phase stratiform clouds from warm clouds in terms of cloud development and its interactions with aerosols, and how this differentiation varies among cases of mixed-phase stratiform clouds with different ICNC/CDNC values. This attempt is valuable, considering that in general, the establishment of the general principle for stratocumulus clouds and their interactions with aerosols has been progressed much less than that for other types of clouds such as convective clouds and their interactions with aerosols. The attempt is valuable, also considering that our level of understanding of how ice processes differentiate mixed-phase stratiform clouds and their interactions with aerosols from much-studied warm clouds and their interactions with aerosols has been low. Here, we want to emphasize that this study does not aim to gain a fully established general principle, but aims to test the factor that can be useful to move ahead on our path to a more complete general principle. Hence, this study should be regarded a steppingstone to the established principle, and should not be considered a perfect study that get us the fully established principle. Taking into account the fact that even attempts to provide general factors for the general principle have been rare, the fulfilment of the aim is likely to provide us with valuable preliminary information that streamlines the development of a more established general principle.

For the attempt, this study investigates a case of mixed-phase stratiform clouds in the polar region. Via the investigation, this study aims to identify process-level mechanisms that control the development of those clouds and their interactions with aerosols, and the impact of ice processes on the development and interactions using a large-eddy simulation (LES) framework. Then, this study compares the mechanisms in the case of polar clouds to those in a case of midlatitude clouds which have been examined by Lee et al. (2021). This comparison is based on Choi et al. (2010 and 2014) and Zhang et al. (2019) which have shown that temperature is an important factor which explains the differences in IWC/LWC among regions or clouds. Due to significant differences in latitudes, noticeable differences in the temperature of air are between the polar and midlatitude cases. Hence, through this comparison, this study looks at the role of temperature in those differences in IWC/LWC and associated aerosol-cloud interactions. More importantly than that, as a way of identifying process-level mechanisms that control the role of temperature, this study tests how ICNC/CDNC as the general factor is linked to the role of temperature, using the LES framework. Through this test, this study also identifies process-level mechanisms that control how ICNC/CDNC affects roles of ice processes in the differentiation between mixed-phase stratiform and warm clouds in terms of cloud development and its interactions with aerosols, and causes the variation of the differentiation between the cases of mixed-phase stratiform clouds.

2. Case, model and simulations

2.1 LES model

LES simulations are performed by using the Advanced Research Weather Research and Forecasting (ARW) model. A bin scheme, which is detailed in Khain et al. (2000) and Khain et al. (2011), is adopted by the ARW for the simulation of microphysics. Size distribution functions for each class of hydrometeors, which are classified into water drops, ice crystals (plate, columnar and branch types), snow aggregates, graupel and hail, are represented with 33 mass doubling bins, i.e., the mass of a particle m_k in the kth bin is determined as $m_k = 2m_{k-1}$. Each of hydrometeors has its own terminal velocity that varies with the hydrometeor mass and the sedimentation of hydrometeors is simulated using their terminal velocity.

Size distribution functions for aerosols, which act as cloud condensation nuclei (CCN) and ice-nucleating particles (INP), adopt the same mass doubling bins as for hydrometeors. The evolution of aerosol size distribution and associated aerosol concentrations at each grid point is controlled by aerosol sinks and sources such as aerosol advection, turbulent mixing, activation and aerosol regeneration via the evaporation of droplets and the sublimation of ice crystals. Aerosol regeneration follows the method similar to that as described in Xue et al. (2010). It is assumed that aerosols do not fall down by themselves and move around by airflow that is composed of horizontal flow, updrafts, downdrafts and turbulent motions. When aerosols move with airflow, it is assumed that they move with the same velocity as airflow. Taking activation as an example of the evolution of aerosol size distribution, the bins of the aerosol spectra that correspond to activated particles are emptied. Activated aerosol particles are included in hydrometeors and move to different classes and sizes of hydrometeors through collision-coalescence. In case hydrometeors with aerosol particles precipitate to the surface, those particles are removed from the atmosphere.

The large energetic turbulent eddies are directly resolved by the LES framework, and the effects of the smaller subgrid-scale turbulent motions on the resolved flow are parameterized based on a most widely used method that Smagorinsky (1963) and Lilly (1967) proposed. In this method, the mixing time scale is defined to be the norm of the strain rate tensor (Bartosiewicz and Duponcheel, 2018). A cloud-droplet nucleation parameterization based on Köhler theory represents cloud-droplet nucleation. Arbitrary aerosol mixing states and aerosol size distributions can be fed to this parameterization. To represent heterogeneous ice-crystal nucleation, the parameterizations by Lohmann and Diehl (2006) and Möhler et al. (2006) are used. In these parameterizations, contact, immersion, condensation-freezing, and deposition nucleation paths are all considered by taking into account the size distribution of INP, temperature and supersaturation. Homogeneous aerosol (or haze particle) and droplet freezing is also considered following the theory developed by Koop et al. (2000).

The bin microphysics scheme is couped to the Rapid Radiation Transfer Model (RRTM; Mlawer et al., 1997). The effective sizes of hydrometeors, which are calculated in the bin scheme, are fed into the RRTM as a way of considering effects of the effective sizes on radiation. The surface process and resultant surface heat fluxes are simulated by the interactive Noah land surface model (Chen and Dudhia, 2001).

2.2 Case and simulations

2.2.1 Case and standard simulations

In the Svalbard area, Norway, a system of mixed-phase stratocumulus clouds existed over the horizontal domain marked by a red rectangle in Figure 1 and a period between 02:00 and 10:00 local solar time (LST) on March 29th, 2017. These clouds are observed by the Cloudnet ground observation that has been established to provide a systematic evaluation of clouds in forecast and climate models. The Cloudnet observation aims to establish a number of ground-based remote sensing sites, which would all be equipped with a specific array of instrumentation, using active sensors such as lidar and Dopplerized mm-wave radar, in order to provide vertical profiles of the main cloud variables (e.g., LWP and IWP), at high spatial and temporal resolution (Hogan et al., 2006). The Cloudnet observation provides data of important cloud variables such as LWP and IWP to the public and this study utilize these data.

On average, the bottom and top of the observed clouds, which are measured by radar and lidar in the Cloudnet observation, are at ~400 m and ~3 km in altitude, respectively. The simulation of the observed system or case, i.e., the control run, is performed three-dimensionally over the red rectangle and the period between 02:00 and 10:00 LST on March 29th, 2017. The horizontal domain adopts a100-m resolution for the control run. The length of the domain in the horizontal directions is 50 km. The length of the domain in the vertical direction is ~5 km and the resolution for the vertical domain gets coarsened with height from ~5 m just above the surface to ~150 m at the model top as detailed in the supplement. Reanalysis data, which are produced by Met Office Unified Model (Brown et al., 2012) every 6 hours on a 0.11° × 0.11° grid, provide potential temperature, specific humidity, and wind as initial and boundary conditions, which represent synoptic-scale environment, for the control run. The control run employs an open lateral boundary condition. Figure 2a shows the vertical distribution of the domain-averaged potential temperature and humidity in those reanalysis data at the first time step. A neutral, mixed layer is between the surface and 1 km in altitude as an initial condition (Figure 2a). Figure 2b shows the time evolution of the domain-averaged large-scale subsidence or downdraft in the reanalysis data and at the model top. This large-scale subsidence is imposed on the control run as a part of background wind fields and interacts with updrafts and downdrafts generated by relatively small-scale processes including those associated with clouds. The large-scale subsidence gradually reduces with time (Figure 2b). Figure 2c shows the time evolution of the domain-averaged surface temperature in the reanalysis data. This evolution of the surface temperature is mostly controlled by the sea surface temperature considering that most portion of the red-rectangle domain is accounted for by the ocean (Figure 1). Due to the sunrise, the surface temperature starts to increase more rapidly around 08:00 LST (Figure 2c).

The properties of cloud condensation nuclei (CCN) such as the number concentration, size distribution and composition are measured in the domain (Tunved et al., 2013; Jung et al., 2018). The measurement of the CCN concentration has been carried out at the Zeppelin research station in the domain, using the commercial droplet measurement technologies CCN counter with one column (CCNC-100), managed by the Korea Polar Research Institute, since year 2007. The CCNC-100 measures the CCN concentration at supersaturations of 0.2, 0.4, 0.6, 0.8 and 1% (Jung et al., 2018). The aerosol number size distribution is observed using a closed-loop differential mobility particle sizer (DMPS). The DMPS charges aerosol particles and exposing them into an electric field, which causes them to experience a force proportional to their electrical mobility, resulting in their classification according to size (Tunved et al., 2013). Aerosol composition is measured using aerosol mass spectrometry (AMS). The AMS measures the composition by vaporizing and ionizing aerosol particles.

The measurement indicates that on average, aerosol particles are an internal mixture of 70 % ammonium sulfate and 30 % organic compound. This mixture is assumed to represent aerosol chemical composition over the whole domain and simulation period for this study. The observed and averaged concentration of aerosols acting as CCN is ~200 cm^{-3} over the simulation period between 02:00 and 10:00 LST on March 29th, 2017. Note that the average of a variable with respect to time in the rest of this paper is performed over this period between 02:00 and 10:00 LST, unless otherwise stated. 200 cm^{-3} as the averaged concentration of aerosols acting as CCN is interpolated into all of grid points immediately above the surface at the first time step.

This study does not take into account aerosol effects on radiation before aerosol is activated, since no significant amount of radiation absorbers is found in the mixture. Based on observation, the size distribution of aerosols acting as CCN is assumed to be a tri-modal log-normal distribution (Figure 3). The shape of distribution, which is a tri-modal log-normal distribution, as shown in Figure 3 is applied to the size distribution of aerosols acting as CCN in all parts of the domain during the whole simulation period. The assumed shape in Figure 3 is obtained by performing the average on the observed size distribution parameters (i.e., modal radius and standard deviation of each of nuclei, accumulation and coarse modes, and the partition of aerosol number among those modes) over the simulation period. Note that although these parameters or the shape of aerosol size distribution does not vary, associated aerosol concentrations vary over the simulation domain and period via processes as described in Section 2.1. This study takes an assumption that the interpolated CCN concentrations do not vary with height in a layer between the surface and the planetary boundary layer (PBL) top around 1 km in altitude at the first time step, following the previous studies such as Gras (1991), Jaenicke (1993) and Seinfeld and Pandis (1998). However, above the PBL top, they are assumed to decrease exponentially with height at the first time step, based on those previous studies, although the shape of size distribution and composition do not change with height. It is assumed that the properties of INP and CCN are not different except for concentrations. The concentration of aerosols acting as CCN is assumed to be 100 times higher than that acting as INP over grid points at the first time step based on a general difference in concentrations between CCN and INP (Pruppacher and Klett, 1978). Hence, the concentration of aerosols acting as INP at the first time step is 2 cm^{-3} in the control run. This assumed concentration of aerosols acting as INP is higher than usual (Seinfeld and Pandis, 1998). However, Hartmann et al. (2021) observed the INP concentration that was at the same order of magnitude as assumed here in the Svalbard area when strong dust events occur, meaning that the assumed INP concentration is not that unrealistic.

To examine effects of aerosols on mixed-phase clouds, the control run is repeated by increasing the concentration of aerosols by a factor of 10. In the repeated (control) run, the initial concentrations of aerosols acting as CCN and INP at grid points immediately above the surface are 2000 (200) and 20 (2) cm^{-3}, respectively. Reflecting these concentrations in the simulation name, the control run is referred to as “the 200_2 run” and the repeated run is referred to as “the 2000_20 run”. To isolate effects of aerosols acting as CCN (INP) on mixed-phase clouds, the control run is repeated again by increasing the concentration of aerosols acting as CCN (INP) only but not INP (CCN) by a factor of 10. In this repeated run with the increase in the concentration of aerosols acting as CCN (INP), the initial concentrations of aerosols acting as CCN and INP at grid points immediately above the surface are 2000 (200) and 2 (20) cm^{-3}, respectively. Reflecting this, the repeated run is referred to as "the 2000_2 (200_20) run".

2.2.2 Additional simulations

To isolate impacts of ice processes on the adopted case and its interactions with aerosols, the 200_2 and 2000_2 runs are repeated by removing ice processes. These repeated runs are referred to as the 200_0 and 2000_0 runs. In the 200_0 and 2000_0 runs, all hydrometeors (i.e., ice crystals, snow, graupel, and hail), phase transitions (e.g., deposition and sublimation) and aerosols (i.e., INP) which are associated with ice processes are removed. Hence, in these runs, only droplets (i.e., cloud liquid), raindrops, associated phase transitions (e.g., condensation and evaporation) and aerosols acting as CCN are present, regardless of temperature. Stated differently, these noice runs simulate the warm-cloud counterpart of the selected mixed-phase cloud system. Via comparisons between a pair of the 200_2 and 2000_2 runs and a pair of the 200_0 and 2000_0 runs, the role of ice processes in the differentiation between mixed-phase and warm clouds is to be identified. Along with this identification, the role of the interplay between ice crystals and droplets in the development of the selected mixed-phase cloud system and its interactions with aerosols is to be isolated.

As detailed in Sections 3.1.4 and 3.2.2 below, the test of ICNC/CDNC as a general factor requires more simulations to see impacts of ICNCavg/CDCNavg on clouds and their interactions with aerosols. Here, ICNCavg and CDNCavg represent the average ICNC and CDNC over grid points and time steps with non-zero ICNC and CDNC, respectively. ICNCavg/CDNCavg represents overall ICNC/CDNC over the domain and simulation period. To respond to this requirement, the 200_0.07, 2000_0.07 and 200_0.7 runs are performed and their details are given in Sections 3.1.4 and 3.2.2. In addition, all the simulations above are repeated by turning off radiative processes and Section 3.3 provides the details of these repeated simulations. These repeated runs are the 200_2_norad, 2000_20_norad, 2000_2_norad, 200_20_norad, 200_0_norad, 2000_0_norad, 200_0.07_norad, 2000_0.07_norad and 200_0.7_norad runs. Moreover, based on the argument in Section 4.2, the 4000_45, 13_0.1, 4000_1.8 and 12_0.0035 runs are performed and details of these runs are provided in Section 4.2. Some of the simulations are summarized in Table 1 for better clarification with a brief description of their configuration.

3. Results

3.1 The 200_2 run vs. the 200_0 run

3.1.1 Model validation

This study adopts the Cloudnet ground observation to evaluate the 200_2 run. Observed LWP is provided by radiometer in the Cloudnet observation. The retrieval of IWP is performed by using radar reflectivity and lidar backscatter in the Cloudnet observation as described in Donovan et al. (2001), Donovan and Lammeren (2001), Donovan (2003) and Tinel et al. (2005). In the retrieval, the lidar signal and radar reflectivity profiles are combined and inverted using a combined lidar/radar equation as a function of the light extinction coefficient and radar reflectivity. The combined equation is detailed in Donovan and Lammeren (2001). Simulated LWP and IWP, as shown in Figure 4 and Table 2, are compared to the observed LWP and retrieved IWP, respectively. The average LWP over all time steps and grid columns for the period between 02:00 and 10:00 LST on March 29th, 2017 is 1.23 g m^{-2} in the 200_2 run and 1.12 g m^{-2} in Cloudnet observation. The average IWP over all time steps and grid columns over the period is 31.94 g m^{-2} in the 200_2 run and 29.10 g m^{-2} in the retrieval. Cloud-bottom height, which is averaged over grid columns and time steps with non-zero cloud-bottom height over the period, is 420 and 440 m in the 200_2 run and Cloudnet observation, respectively. Cloud-top height, which is averaged over grid columns and time steps with non-zero cloud-top height over the period, is 3.5 and 3.3 km in the 200_2 run and Cloudnet observation, respectively. Each of LWP, cloud-bottom and -top heights shows an ~10% difference between the 200_2 run and observation.

IWP also shows an ~10% difference between the 200_2 run and the retrieval. Thus, the 200_2 run is considered performed reasonably well for these variables.

To provide additional information of cloud development, Figure 5 shows the time evolution of the simulated and observed cloud-top and bottom heights, simulated and retrieved IWP and simulated and observed LWP together with the evolution of the simulated surface sensible and latent-heat fluxes; the simulated evolutions in Figure 5 are from the 200_2 run. This is based on the fact that the cloud-top and bottom heights, IWP and LWP are considered a good indicative of cloud development and the surface fluxes are considered important parameters controlling the overall development of clouds. The cloud-top height increases between 02:00 and ~05:00 LST and after ~05:00 LST, it reduces gradually. The cloud-bottom height decreases between 02:00 and ~05:00 LST and after ~05:00 LST, it does not change much. IWP and LWP show an overall increase between 02:00 and ~05:30 LST to reach its peak around 05:30 LST and then an overall decrease. The surface fluxes reduce with time, although the reduction rate of the fluxes starts to decrease around 08:00 LST in association with the rapid increase in the surface temperature which starts around 08:00 LST as shown in Figure 2c.

The time- and domain-averaged IWP and IWC are ~one order of magnitude greater than LWP and LWC, respectively, in the 200_2 run (Figure 4 and Table 2). For the sake of simplicity, the averaged IWC over the averaged LWC is denoted by IWC/LWC, and the averaged IWP over the averaged LWP is by IWP/LWP, henceforth. IWC/LWC and IWP/LWP are 26.28 and 25.96, respectively, in the 200_2 run. Since IWP and LWP are vertically integrated IWC and LWC over the vertical domain, respectively, the qualitative nature of differences between IWC and LWC is not much different from that between IWP and LWP. Hence, mentioning both a pair of IWC and LWC and that of IWP and LWP is considered redundant, and mentioning either a pair of IWC and LWC or that of IWP and LWP enhances the readability. Henceforth, IWC and LWC are chosen to be mentioned in text, although all of IWC, LWC, IWP and LWP are displayed in Tables 2 and 3.

Choi et al. (2014) and Zhang et al. (2019) have obtained the supercooled cloud fraction (SCF), which is basically the ratio of LWC to the sum of LWC and IWC and denoted by LWC/(LWC+IWC), using satellite- and ground-observed data collected over the period of ~5 years and ~1 year, respectively. Choi et al. (2014) have shown that SCF is as low as

~0.01 for the temperature range between -16 and -33 ºC. Zhang et al. (2019) have also shown that SCF is as low as ~0.03 for the same temperature range, although the occurrence of SCF of ~0.03 or lower is rare. Note that the average air temperature immediately below the cloud base and above the cloud top over the simulation period is -16 and -33 ºC, respectively, in the 200_2 run, and SCF in the 200_2 run is 0.04. Hence, based on Choi et al. (2014) and Zhang et al. (2019), we believe that SCF in the 200_2 run is observable and thus not that unrealistic, although it may not occur frequently.

3.1.2 Microphysical processes, sedimentation and entrainment

To understand process-level mechanisms that control the results, microphysical processes are analyzed. As indicated by Ovchinnikov et al. (2011), in clouds with weak precipitation, a high-degree correlation is found between IWC and deposition or between LWC and condensation, considering that deposition and condensation are sources of IWC and LWC, respectively. In the 200_2 run, the average surface precipitation rate over the simulation period is ~0.0020 mm hr^{-1}, which can be considered weak. Hence, in this case, condensation and deposition are considered proxies for LWC and IWC, respectively. Based on this, to gain a process-level understanding of microphysical processes that control the simulated LWC and IWC, condensation and deposition are analyzed.

As seen in Figure 6 and Table 2, the average deposition rate is ~one order of magnitude greater than condensation rate in the 200_2 run, leading to much greater IWC than LWC in the 200_2 run. This is in contrast to the situation in the case of mixed-phase stratocumulus clouds, which were located in a midlatitude region, in Lee et al. (2021). In that case, the average IWC and LWC are at the same order of magnitude. For the sake of brevity, the case in Lee et al. (2021) is referred to as “the midlatitude case”, while the case of mixed-phase clouds, which is adopted by this study, in the Svalbard area is referred to “the polar case”, henceforth. In the midlatitude case, IWC/LWC is 1.55, which is ~ one order of magnitude smaller than that in the polar case.

Warm clouds in the 200_0 run shows that the time- and domain-averaged condensation rate that is lower than the time- and the domain-averaged sum of condensation and deposition rates in the 200_2 run (Figure 6 and Table 2). This leads to a situation where warm clouds in the 200_0 run shows the time- and domain-averaged LWC that is lower than the time- and domain-averaged water content (WC), which is the sum of IWC and LWC, in mixed-phase clouds in the 200_2 run (Figure 4 and Table 2). This is despite the fact that LWC in the 200_0 run is higher than LWC in the 200_2 run (Figure 4 and Table 2); WC represents the total cloud mass in mixed-phase clouds, while LWC alone represents the total cloud mass in warm clouds.

It should be noted that the average rate of sedimentation of droplets over the cloud base and simulation period reduces from the 200_0 run to the 200_2 run (Table 2). This is mainly due to the decrease in LWC from the 200_0 run to the 200_2 run. The average rate of sedimentation of ice crystals over the cloud base and simulation period increases from the 200_0 run to the 200_2 run, since sedimentation of ice crystals is absent in the 200_0 run (Table 2). The average entrainment rate over the cloud top and simulation period increases from the 200_0 run to the 200_2 run (Table 2). Here, entrainment rate is defined to be the difference between the rate of increase in cloud-top height and the large-scale subsidence, following Moeng et al. (1999), Jiang et al. (2002), Stevens et al. (2003a and 2003b) and Ackerman et al. (2004). Entrainment tends to reduce the total cloud mass more in the 200_2 run than in the 200_0 run. Thus, entrainment should be opted out when it comes to mechanisms leading to the increase in the total cloud mass from the 200_0 run to the 200_2 run. Here, the vertical integration of each of condensation and deposition rates is obtained over each cloudy column in the domain for each of the runs. For the sake of the brevity, this vertical integrations of condensation and deposition rates are referred to as the integrated condensation and deposition rates, respectively. Then, each of the integrated condensation and deposition rates is averaged over cloudy columns and the simulation period. It is found that the average rates of the droplet and ice-crystal sedimentation over the cloud base and simulation period are ~four orders of magnitude smaller than the average integrated condensation and deposition rates, respectively, in the 200_2 run (Table 2). It is also found that the average rate of the droplet sedimentation over the cloud base and simulation period is ~five orders of magnitude smaller than that in the average integrated condensation rate in the 200_0 run (Table 2). Changes in the average rates of the droplet and ice-crystal sedimentation over the cloud base and simulation period are ~four to five orders of magnitude smaller than those in the average integrated condensation and deposition rates between the 200_2 and 200_0 runs (Table 2). Thus, condensation and deposition, but not the droplet and ice-crystal sedimentation, are main factors controlling cloud mass, which is represented by LWC and IWC, and the total cloud mass in the 200_2 and 200_0 runs, and the variation of cloud mass and the total cloud mass between the runs as are in the midlatitude case and its warm-cloud counterpart.

3.1.3 Hypothesis

We hypothesized that ICNC/CDNC can be an important factor that determines above-described differences between the polar and midlatitude cases. Note that both in the polar and midlatitude cases, pockets of ice particles and those of liquid particles are mixed together instead of being separated from each other as seen in Figure 4 and Lee et al. (2021). Remember that ice crystals are more as sources of deposition per a droplet when ICNC/CDNC is higher. Thus, when ICNC/CDNC is higher and $qv > qsw$, it is more likely that more portion of water vapor is deposited onto ice crystals by stealing water vapor, which is supposed to be condensed onto droplets, from droplets in an air parcel. Here, qv and qsw represent water-vapor pressure and water-vapor saturation pressure for liquid water or droplets, respectively. When ICNC/CDNC is higher and $qsi < qv < qsw$, more ice crystals can absorb water vapor, including that which is produced by droplet evaporation, per a droplet; here, qsi represents water-vapor saturation pressure for ice water or ice crystals. Thus, with higher ICNC/CDNC, it is more likely that more portion of water vapor is deposited onto ice crystals in an air parcel as shown in Lee et al. (2021). Figure 7 shows the time series of the averaged supersaturation over gird points where deposition occurs in the presence of both droplets and ice crystals in the 200_2 run. Figure 7 indicates that on average, supersaturation occurs for both droplets and ice crystals over those grid points. Hence, on average, the above-described situation of $qv > qsw$ is applicable to deposition when droplets and ice crystals coexist in the 200_2 run.

ICNCavg/CDNCavg is 0.22 in the control run (i.e., the 200_2 run) for the polar case and 0.019 in the control run for the midlatitude case which is described in Lee et al. (2021). Henceforth, the control run for the midlatitude case is referred to as the control-midlatitude run. ICNCavg/CDNCavg is ~one order of magnitude higher for the polar case than for the midlatitude case. This is despite the fact that the ratio of the initial number concentration of aerosols acting as INP to that of acting as CCN is identical between the 200_2 and control-midlatitude runs. In addition, identical model, model setup such as vertical resolutions, and source of reanalysis data are used between the 200_2 and control-midlatitude runs, although there are differences in environmental conditions (e.g., temperature), cloud macrophysical variables such as cloud-top height and horizontal resolutions between the runs. Here, while taking these similarities and differences into account, we hypothesize that the significant differences in ICNCavg/CDNCavg between runs are mainly due to the fact that ice nucleation strongly depends on air temperature (Prappucher and Klett, 1978). When supercooling is stronger, in general, more ice crystals are nucleated for a given group of aerosols acting as INP. The average air temperature immediately below the cloud base over the simulation period is -16 ºC in the 200_2 run and -5 ºC in the control-midlatitude run. The average air temperature immediately above the cloud top is -33 ºC in the 200_2 run and -15 ºC in the control-midlatitude run. Hence, supercooling is greater and this contributes to the higher ICNCavg/CDNCavg in the polar case than in the midlatitude case. The higher ICNCavg/CDNCavg is likely to induce more portion of water vapor to be deposited onto ice crystals in the polar case than in the midlatitude case. It is hypothesized that this in turn enables IWC/LWC in the 200_2 run to be one order of magnitude greater than that in the control-midlatitude run or in the midlatitude case. Much higher IWC than LWC, which results in a much higher IWC/LWC in the polar case than in the midlatitude case, in the 200_2 run overcomes lower LWC in the 200_2 run than that in the 200_0 run, which leads to the greater total cloud mass in the 200_2 run than in the 200_0 run (Figure 4 and Table 2). However, IWC whose magnitude is similar to the magnitude of LWC, which results in a much lower IWC/LWC in the midlatitude case than in the polar case, in the midlatitude case is not able to overcome lower LWC in the midlatitude case than that in the midlatitude warm clouds, which leads to the greater total cloud mass in the midlatitude warm clouds than in the midlatitude case; here, the midlatitude warm clouds are generated by removing ice processes in the midlatitude case. This means that associated with higher ICNC/CDNC and IWC/LWC, ice processes enhance the total cloud mass for the polar case as compared to that for the polar warm-cloud counterpart. However, in the midlatitude case, associated with lower

ICNC/CDNC and IWC/LWC, ice processes reduce the total cloud mass as compared to that for the midlatitude warm-cloud counterpart.

3.1.4 Role of ICNC/CDNC

To test the hypothesis above about the role of ICNC/CDNC in above-described differences between the polar and midlatitude cases, the 200_2 run is repeated by reducing ICNCavg/CDNCavg by a factor of 10. This is done by reducing the concentration of aerosols acting as INP but not CCN in a way that ICNCavg/CDNCavg is lower by a factor of 10 in the repeated run than in the 200_2 run. In this way, this repeated run has ICNCavg/CDNCavg at the same order of magnitude as that in the control-midlatitude run. This repeated run is referred to as the 200_0.07 run. As shown in Figure 8 and Table 2, the 200_0.07 run shows much lower deposition rate and IWC than the 200_2 run does. However, as we move from the 200_2 run to the 200_0.07 run, the time- and domain-averaged condensation rate and LWC increases (Figure 8 and Table 2). This is because reduction in deposition increases the amount of water vapor, which is not consumed by deposition but available for condensation. Associated with this, in the 200_0.07 run, the time- and domain-averaged deposition rate and IWC become similar to the average condensation rate and LWC, respectively (Figure 8 and Table 2). Hence, IWC/LWC reduces from 26.28 in the 200_2 run to 1.05 in the 200_0.07 run as ICNCavg/CDNCavg reduces from the 200_2 run to the 200_0.07 run. Here, IWC/LWC in the 200_0.07 run is similar to that in the midlatitude-control run, which demonstrate that the difference in ICNC/CDNC is able to explain the difference in IWC/LWC between the polar and midlatitude cases. It is notable that the reduction in deposition is dominant over the increase in condensation with the decrease in ICNCavg/CDNCavg. Hence, the sum of condensation and deposition rates and WC reduce from the 200_2 run to the 200_0.07 run. That the sum of condensation and deposition rates and WC reduce in a way that the sum and WC in the mixed-phase clouds in the 200_0.07 run are lower than condensation rate and LWC, respectively, in the warm clouds in the 200_0 run is also notable (Figure 8 and Table 2). This is similar to the situation in the midlatitude case and thus demonstrates that the different relation between the mixed-phase and warm clouds can be associated with the difference in ICNC/CDNC between the polar and midlatitude cases.

The rate of the sedimentation of ice crystals at the cloud base reduces as ICNCavg/CDNCavg reduces between the 200_2 and 200_0.07 runs, mainly due to reduction in the ice-crystal mass (Table 2). The rate of droplet sedimentation at the cloud base increases as ICNCavg/CDNCavg reduces mainly due to increases in droplet mass and size in association with the increases in LWC (Table 2). The entrainment rate at the cloud top reduces as ICNCavg/CDNCavg reduces (Table 2). It is found that those changes in the average rates of the droplet and ice-crystal sedimentation over the cloud base and simulation period are ~four to five orders of magnitude smaller than those in the average integrated condensation and deposition rates between the 200_2 and 200_0.07 runs (Table 2). The entrainment tends to reduce the total cloud mass or WC less with the reducing ICNCavg/CDNCavg. Hence, changes in the entrainment counters the decrease in WC with the reducing ICNCavg/CDNCavg between the 200_2 and 200_0.07 runs. Here, we see that changes in the entrainment are not factors that lead to the increase in LWC, and the decrease in IWC, and eventually the decrease in WC with the reducing ICNCavg/CDNCavg. The analysis of the sedimentation and entrainment exclude them from factors inducing above-described differences between the 200_2 and 200_0.07 runs. Instead, this analysis grants confidence in the fact that deposition and condensation, which are strongly dependent on ICNC/CDNC, are main factors inducing those differences.

3.2 Aerosol-cloud interactions

Comparisons between the 200_2 and 2000_20 runs show that with the increasing concentration of both of aerosols acting as CCN and those as INP, IWC increases but LWC decreases in the polar case (Figures 9 and Table 2). These decreases in LWC are negligible as compared to these increases in IWC. Hence, the increases in IWC outweigh the decreases in LWC, leading to aerosol-induced increases in WC (Figures 9 and Table 2). To identify roles of specific types of aerosols in these aerosol-induced changes, comparisons not only between the 200_2 and 200_20 runs but also between the 200_2 and 2000_2 runs are performed. Comparisons between the 200_2 and 200_20 runs show that the increasing concentration of aerosols acting as INP induces increases in IWC but decreases in LWC (Figure 9 and Table 2). The magnitudes of these increases and decreases are similar to those between the 200_2 and 2000_20 runs (Figure 9 and Table 2). However, comparisons between the 200_2 and 2000_2 runs show that the increasing concentration of aerosols acting as CCN induces negligible changes in either IWC or LWC. Thus, CCN-induced changes in the total cloud mass are negligible, although the increasing concentration of aerosols acting as CCN induces a slight decrease in IWC, and a slight increase in LWC (Figure 9 and Table 2). This demonstrates that INP plays a much more important role than CCN when it comes to the response of the total cloud mass to increasing aerosol concentrations. However, in the midlatitude case, the increasing concentration of aerosols acting as CCN generates changes in the mass as significantly as the increasing concentration of aerosols acting as INP does.

To identify roles played by ice processes in aerosol-cloud interactions, a pair of the 200_0 and 2000_0 runs are analyzed and compared to the previous four standard simulations (i.e., the 200_2, 200_20, 2000_2 and 2000_20 runs). The CCN-induced increases in LWC in those noice runs are much greater than the CCN-induced changes in WC in the 200_2 and 2000_2 runs (Figure 9 and Table 2). However, these CCN-induced increases in LWC in the noice runs are smaller than the INP-induced increases in WC in the 200_2 and 200_20 runs (Figure 9 and Table 2). This is different from the midlatitude case where changes in the total cloud mass, whether they are induced by the increasing concentration of aerosols acting as CCN or INP, in the mixed-phase clouds are much lower than those CCN-induced changes in the warm clouds.

3.2.1 Deposition, condensation, sedimentation and entrainment

The CCN-induced increases and decreases in condensation and deposition rates are negligible, respectively. This leads to the CCN-induced negligible increases and decreases in LWC and IWC, respectively, between the 200_2 and 2000_2 runs (Figure 9 and Table 2). However, between the 200_2 and 200_20 runs, rather the significant INP-induced increases are in deposition rate, leading to the significant INP-induced increases in IWC (Figure 9 and Table 2). Between the 200_2 and 200_20 runs, INP-induced decreases in condensation rate are negligible, leading to the negligible INP-induced decreases in LWC, as compared to the INP-induced increases in deposition rate and IWC (Figure 9 and Table 2). With the increasing concentration of aerosols acting as INP from the 200_2 run to the 200_20 run, the sedimentation of ice crystals at the cloud base decreases (Table 2). This is mainly due to decreases in the size of ice crystals in association with increases INP and resultant increases in ICNC. In Figure 10a, we see that the number concentration of ice crystals with diameters smaller and larger than ~40 micron increases and decreases, respectively, as we move from the 200_2 run to the 200_20 run, which indicate a shift of the sizes of ice crystals to smaller ones. From the 200_2 run to the 200_20 run, the sedimentation of droplets at the cloud base decreases as shown in Table 2, mainly due to decreases in LWC. Figure 10b shows that the number concentration of drops decreases throughout almost all parts of the size range from the 200_2 run to the 200_20 run, which indicates a negligible shift in the drop size but a reduction in LWC. It is found that changes in the average rates of the droplet and ice-crystal sedimentation over the cloud base and simulation period are ~three to four orders of magnitude smaller than those in the average integrated condensation and deposition rates between the 200_2 and 200_20 runs (Table 2). From the 200_2 run to the 200_20 run, the entrainment at the cloud top increases (Table 2). Hence, the entrainment reduces WC less in the 200_2 run than in the 200_20 run. Here, we see that changes in entrainment and the sedimentation are not factors that we have to focus on to explain the changes in LWC, IWC and WC between the 200_2 and 200_20 runs.

In the warm clouds in the 200_0 and 2000_0 runs, the CCN-induced increases in condensation rate occur, leading to those in LWC (Figure 9 and Table 2). However, the CCN-induced increases in condensation rate in the warm clouds associated with the polar case are lower than the INP-induced increases in deposition rate in the polar case (Table 2). This contributes to aerosol-induced smaller changes in the total cloud mass in the polar warm clouds than in the polar mixed-phase clouds. The sedimentation of droplets at the cloud base reduces and the entrainment at the cloud top increases from the 200_0 run to 2000_0 run (Table 2). The increasing concentration of aerosols acting as CCN induces increases in CDNC and decreases in the droplet size, leading to the reduction in the droplet sedimentation from the 200_0 run to 2000_0 run. The entrainment counters the CCN-induced increases in LWC from the 200_0 run to 2000_0 run. Hence, the entrainment is not a factor which induces the CCN-induced increases in LWC between the 200_0 and 2000_0 runs. As seen in Table 2, the changes in the sedimentation rate is ~three orders of magnitude smaller than those in the integrated condensation rate between the 200_0 and 2000_0 runs. Hence, it is not the sedimentation but condensation that we have to look at to explain changes in LWC or WC between the 200_0 and 2000_0 runs.

3.2.2 Understanding differences between the polar and midlatitude cases

Roughly speaking, the CCN-induced changes in LWC via CCN-induced changes in autoconversion of droplets are proportional to LWC that changing CCN affect, and INP-induced changes in IWC via INP-induced changes in autoconversion of ice crystals are proportional to IWC that changing INPs affect (e.g., Dudhia, 1989; Murakami, 1990; Liu and Daum, 2004; Morrison et al., 2005, 2009 and 2012; Lim and Hong, 2010; Mansell et al. 2010; Kogan, 2013; Lee and Baik, 2017). This is for given environmental conditions (e.g., temperature and humidity) and given CCN- or INP-induced changes in microphysical factors such as sizes and number concentrations of droplets or ice crystals. Hence, in the polar case, with a given much lower LWC than IWC, the changing concentration of aerosols acting as CCN is likely to induce smaller changes in the given LWC via CCN impacts on the droplet autoconversion. This is as compared to changes in the given IWC which are induced by the changing concentration of aerosols acting as INP and thus changing ice-crystal autoconversion.

The smaller changes in the given LWC are related to changes in CDNC. These changes in CDNC are initiated by those in droplet autoconversion. The larger changes in the given IWC are related to changes in ICNC. These changes in ICNC are initiated by those in ice-crystal autoconversion. Changes in integrated droplet surface area, which are induced by those in CDNC, initiate those in the given LWC. Changes in integrated ice-crystal surface area, which are induced by those in ICNC, initiate those in the given IWC. Remember that condensation occurs on droplet surface and thus droplets act as a source of condensation, and deposition occurs on ice-crystal surface and thus ice crystals act as a source of deposition. Hence, those changes in CDNC and associated integrated droplet surface area can lead to changes in condensation and thus feedbacks between condensation and updrafts, while those changes in ICNC and associated integrated ice-crystal surface area can lead to changes in deposition and thus feedbacks between deposition and updrafts. The smaller CCN-induced changes in LWC involve changes in CDNC and associated smaller changes in condensation and feedbacks between condensation and updrafts in the polar case. This is as compared to changes in deposition and feedbacks between deposition and updrafts which are associated with the INP-induced changes in ICNC and the related larger INP-induced changes in IWC in the polar case. The smaller CCN-induced changes in LWC involve smaller changes in water vapor that is consumed by droplets in the polar case. The larger INP-induced changes in IWC involve larger changes in water vapor that is consumed by ice crystals in the polar case. This leaves the CCN-induced smaller changes in the amount of water vapor available for deposition, which induce the smaller CCN-induced changes in IWC in the polar case. This is as compared to the INP-induced changes in the amount of water vapor which is available for condensation and associated changes in LWC in the polar case.

The lower LWC in the polar warm clouds than IWC in the polar case contributes to the INP-induced greater changes in IWC than the CCN-induced changes in LWC in the polar warm clouds. The lower LWC in the polar case than that in the polar warm clouds contributes to the CCN-induced greater changes in LWC in the polar warm clouds than those in LWC and subsequent changes in IWC in the polar case.

In contrast to the situation in the polar case, in the midlatitude case, remember that a given LWC is at the same order of magnitude of IWC. Hence, the CCN- induced changes in LWC and subsequent changes in IWC are similar to the INP-induced changes in IWC and subsequent changes in LWC. The greater LWC in the midlatitude warm cloud than both of LWC and IWC in the midlatitude case contributes to the greater CCN-induced changes in LWC in the midlatitude warm cloud. This is as compared to either the CCN-induced changes in LWC and subsequent changes in IWC or the INP-induced changes in IWC and subsequent changes in LWC in the midlatitude case.

To confirm above-described mechanisms in this section, which explain different aerosol-cloud interactions between the polar and midlatitude cases, the 200_0.07 run is repeated by increasing INP by a factor of 10 in the PBL at the first time step. This repeated run is referred to as “the 200_0.7 run. Then, the 200_0.07 run is repeated again by increasing CCN by a factor of 10 in the PBL at the first time step. This repeated run is referred to as the 2000_0.07 run. These repeated runs are to see the response of IWC and LWC to the increasing concentration of aerosols acting as INP and CCN. This is when IWC and LWC are at the same order of magnitude and lower in mixed-phase clouds than LWC in the warm-cloud counterpart as in the 200_0.07 run and midlatitude case. Comparisons between the 200_0.07, 200_0.7 and 2000_0.07 runs show that the INP-induced changes in IWC and LWC are similar to the CCN-induced changes in IWC and LWC, respectively, as in the midlatitude case (Figure 9 and Table 2). These comparisons also show that the CCN-induced changes in LWC in the polar warm cloud are greater (Figure 9 and Table 2). This is as compared to either the CCN-induced changes in LWC and subsequent changes in IWC between the 200_0.07 and 2000_0.07 runs or the INP-induced changes in IWC and subsequent changes in LWC between the 200_0.07 and 200_0.7 runs (Figure 9 and Table 2). These comparisons demonstrate that differences in ICNC/CDNC play a critical role in differences in aerosol-cloud interactions between the polar and midlatitude cases, considering that differences in ICNC/CDNC between the 200_2 and 200_0.07 runs are at the same order of magnitude of those between the cases.

3.3 Radiation

Studies (e.g., Ovchinnikov et al., 2011; Possner et al., 2017; Solomon et al., 2018) have focused on radiative cooling and subsequent changes in stability and dynamics as a primary driver for the development of mixed-phase stratocumulus clouds and aerosol-induced changes in LWC and IWC in those clouds. Motivated by these studies, to isolate the role of radiative processes in cloud development and aerosol impacts on LWC and IWC, all of the simulations above are repeated by turning off radiative processes. In these repeated runs, radiative fluxes over the whole domain and simulation period are zero. The basic summary of results from these repeated runs is given in Table 3. As seen in comparisons between Tables 2 and 3, the qualitative nature of results, which are mainly about differences in IWC/LWC, the relative importance of the impacts of INP on IWC and LWC as compared to those impacts of CCN, and how warm and mixed-phase clouds are related between the polar and midlatitude cases, in this study does not vary with whether radiative processes exist or not. This demonstrates that ICNC, CDNC, deposition and condensation but not radiative processes drive results in this study.

4. Discussion

4.1 Examination of the role of ICNC/CDNC in IWC/LWC in 200_2, 2000_20, 2000_2, 200_20, 200_0.07, 2000_0.07 and 200_0.7 runs

So far, comparisons between the set of the 200_2, 2000_20, 2000_2 and 200_20 runs for the polar case and the other set of the 200_0.07, 2000_0.07 and 200_0.7 runs, which represents the midlatitude case, have been mainly utilized to understand the role of ICNC/CDNC. However, even when it comes to all the runs in both the sets, differences in ICNCavg/CDNCavg and IWC/LWC are shown among them (Tables 1 and 2). For more robust examination of particularly the role of ICNC/CDNC in IWC/LWC, which is basically about the increase and decrease in ICNC/CDNC inducing the increase and decrease in IWC/LWC, respectively, as identified from the comparison between the 200_2 and 200_0.07 runs in Section 3.1.4, all the runs in the sets are utilized by ordering them as shown in Table 4. This ordering is done in a way that as we move from the first run in the first row to the last run in the last row of Table 4, ICNCavg/CDNCavg increases. Overall, with increasing ICNCavg/CDNCavg, IWC/LWC increases, although the increase in IWC/LWC is highly non-linear in terms of the increase in ICNCavg/CDNCavg as seen in the percentage increases, and a decrease in IWC/LWC is seen with an increase in ICNCavg/CDNCavg from the 2000_20 run to the 200_2 run (Table 4); this high-degree non-linearity in the increase in IWC/LWC is associated with the fact that interactions between cloud microphysical, thermodynamic and dynamic processes are well known to be highly non-linear. Hence, overall, findings regarding the role of ICNC/CDNC in IWC/LWC from the comparison between the 200_2 and 200_0.07 runs are applicable to all the runs in the sets except for the role between the 2000_20 and 200_2 runs. Here, it is notable that the percentage difference in ICNCavg/CDNCavg is ~9% between the 2000_20 and 200_2 runs and the smallest among those differences in Table 4. The other differences are larger than 80%. Hence, the percentage difference in ICNCavg/CDNCavg for a pair of the 2000_20 and 200_2 runs is at least ~one order of magnitude smaller than that for the other pairs of the runs in Table 4. This means that findings from the comparison between the 200_2 and 200_0.07 runs are not suitable to explain the variation of IWC/LWC among clouds when the variation of ICNC/CDNC is relatively insignificant. According to Table 4, it seems that the variation of ICNC/CDNC should be greater than a critical value above which those findings are useful to account for the IWC/LWC variation among clouds.

The high-degree non-linearity in the variation of IWC/LWC is epitomized by the 1706 percent increase in IWC/LWC for the 163 percent increase in ICNCavg/CDNCavg from the 200_0.7 run to the 2000_2 run. This 1706 percent increase in IWC/LWC is induced by increases in both the initial number concentrations of CCN and INP between the runs (Table 1). In other transition from a simulation in a row to that in the next row in Table 4, there are decreases in both the initial number concentrations of CCN and INP, or there is either a change in the initial number condensation of CCN or INP. When either the initial concentration of CCN or INP changes in the transition, less than a 100% increase in IWC/LWC is shown. The decreases in both the initial number concentrations of CCN and INP, which are from the 2000_20 run to the 200_2 run, result in the decrease in IWC/LWC. Hence, depending on how the initial number concentrations of CCN and INP change, the magnitude and sign of the change in IWC/LWC can vary substantially.

4.2 Role of a given ICNC/CDNC in IWC/LWC for different concentrations of aerosols acting as INP and CCN

Simulations which are compared in Section 4.1 and shown in Table 4 have not only different ICNCavg/CDNCavg but also the different number concentrations of aerosols acting as CCN and INP at the first time step (Table 1). To better isolate particularly the role of ICNC/CDNC in IWC/LWC, we need to show that results in Section 4.1 are valid regardless of the variation of the number concentration of aerosols. For this need, we focus on the 200_2 and 200_0.07 runs, since the primary understanding of the role of ICNC/CDNC in IWC/LWC comes from the comparison between these runs as described in Section 3.1.4. To fulfill the need, each of these runs are repeated by varying the number concentration of aerosols acting as CCN and INP in a way that ICNCavg/CDNCavg does not vary (Tables 1 and 5). The 4000_45 and 13_0.1 runs are the repeated 200_2 run, and the 4000_1.8 and 12_0.0035 runs are the repeated 200_0.07 run (Tables 1 and 5). The set of the 200_2, 4000_45 and 13_0.1 runs is referred to as the polar set, and that of the 200_0.07, 4000_1.8 and 12_0.0035 runs is referred to as the midlatitude set in this section. Among the three runs in each of the sets, less than 4% variation of IWC/LWC is shown (Table 5). This less-than-4% variation is so small that the start contrast in IWC/LWC between the 200_2 and 200_0.07 runs as discussed in Section 3.1.4 is also shown between the polar and midlatitude sets (Table 5). Hence, the role of the difference in a given ICNC/CDNC in the difference in IWC/LWC between the 200_2 and 200_0.07 runs as described in Section 3.1.4 is considered robust to the varying concentration of aerosols.

5. Summary and conclusions

In this study, a case of mixed-phase stratiform clouds in a polar area, which is referred to as "the polar case" is compared to that in a midlatitude area, which is referred to as "the midlatitude case". This is to gain an understanding of how different ICNC/CDNC plays a role in making differences in cloud properties, aerosol-cloud interactions and impacts of ice processes on them between two representative areas (i.e., polar and midlatitude areas) where mixed-phase stratiform clouds form and develop. Among those cloud properties, this study focuses on IWC/LWC that plays an important role in cloud radiative properties. To gain the understanding efficiently, the polar case is chosen in a way to make stark contrast with the midlatitude case in terms of ICNC/CDNC and IWC/LWC. Although such polar cases may be uncommon, the stark contrast provides an opportunity to elucidate mechanisms that control the above-mentioned role of different ICNC/CDNC.

Due to lower air temperature, more ice crystals are nucleated, leading to higher ICNC/CDNC in the polar case than in the midlatitude case. This higher ICNC/CDNC enables the more efficient deposition of water vapor onto ice crystals in the polar case. This leads to much higher IWC/LWC in the polar case. The more efficient deposition of water vapor onto ice crystals enables the polar mixed-phase clouds to have the greater total cloud mass than the polar warm clouds. However, the less efficient deposition of water vapor onto ice crystals causes the midlatitude mixed-phase clouds to have less total cloud mass than the midlatitude warm clouds. With the increasing ICNC/CDNC from the midlatitude case to the polar case, impacts of CCN and INP on the total cloud mass become less and more important, respectively.

This study picks ICNC/CDNC, which is affected by air temperature and its impacts on ice-crystal nucleation, as an important factor which differentiates IWC/LWC and interactions among clouds, aerosols and ice processes in the polar case from those in the midlatitude case. The polar case is located in the Svalbard area, which is in the Arctic, hence, more specifically, the polar case can be referred to as the Arctic case. Differences in ICNC/CDNC initiate differences in the microphysical properties (e.g., the integrated surface area), and then, subsequently induce those in thermodynamic latent-heat processes (e.g., condensation and deposition), dynamics of clouds, IWC/LWC and interactions among clouds, aerosols and ice processes. However, this does not mean that no other potential factors, which can explain the variation of IWC/LWC and interactions among clouds, aerosols and ice processes between different clouds, exist. For example, differences in environmental factors (e.g., stability and wind shear) between those different clouds can have an impact on the variation. Particularly, differences in stability and wind shear can initiate those in the dynamic development of turbulence. Then, this subsequently induces differences in the microphysical and thermodynamic development of clouds, IWC/LWC and interactions among clouds, aerosols and ice processes. Hence, factors such as stability and wind shear can have different orders of procedures, which involve dynamics, thermodynamics and microphysics, than ICNC/CDNC in terms of differentiation between different clouds. Thus, different mechanisms controlling the differentiation can be expected regarding factors such as stability and wind shear as compared to ICNC/CDNC. The examination of these different mechanisms among stability, wind shear and ICNC/CDNC deserves future study for more comprehensive understanding of the differentiation or for an above-mentioned more fully established general principle explaining the differentiation. Another point to make is that the cases in this study have weak precipitation and the associated weak sedimentation of ice crystals and droplets. In mixed-phase clouds with strong precipitation and the sedimentation, they can play roles as important as in-cloud latent-heat processes in IWC/LWC and interactions among clouds, aerosols and ice processes. In those clouds with strong precipitation, the sedimentation can take part in the interplay between ICNC/CNDC and latent-heat processes by affecting cloud mass and associated ICNC and CDNC significantly, and play a role in the differentiation of IWC/LWC and interactions among clouds, aerosols and ice processes when it comes to different cases of mixed-phase clouds. For more generalization of results here as a way to the more fully established general principle, this potential role of sedimentation needs to be investigated by performing more case studies involving cases with strong precipitation in the future.

It should be emphasized that although this study mentions air temperature as a factor that affects ICNC/CDNC, ICNC/CDNC can be affected by other factors such as sources of aerosols acting as INP and those acting as CCN, and/or the advection of those aerosols. Hence, even for cloud systems that develop with a similar air-temperature condition, for example, when those systems are affected by different sources of aerosols and/or their different advection, they are likely to have different ICNC/CDNC, IWC/LWC, relative importance of impacts of INP on IWC and LWC as compared to those impacts of CCN, and relation between warm and mixed-phase clouds. Regarding factors, which affect ICNC/CDNC, such as sources and advection of aerosols together with temperature , it should be noted that while this study utilizes differences in temperature among those factors to identify cases exhibiting significant disparities in ICNC/CDNC, its primary objective does not lie in the role of temperature differences in disparities in ICNC/CDNC, but in comprehending the inherent role of ICNC/CDNC variations themselves in the discrepancies observed, for example, in IWC/LWC, across diverse cloud systems.

Previous studies on mixed-phase stratocumulus clouds (e.g., Ovchinnikov et al., 2011; Possner et al., 2017; Solomon et al., 2018) have primarily focused on investigating the impacts of cloud-top radiative cooling, entrainment, and sedimentation of ice particles on these clouds, as well as their interactions with aerosols. However, there are a scarcity of studies that specifically examine the role of microphysical interactions, involving processes such as condensation and deposition, as well as factors like cloud-particle concentrations, between ice and liquid particles in mixed-phase stratocumulus clouds, and their interactions with aerosols as performed in this study. Therefore, our study contributes to a more comprehensive understanding of mixed-phase clouds and their intricate interplay with aerosols.

This study suggests that a microphysical factor, which is ICNC/CDNC, can be a simplified and useful tool to understand differences among different systems of stratocumulus clouds in various regions in terms of IWC/LWC and the relative importance of INP and CCN in aerosol-cloud interactions, and thus to contribute to the development of general parameterizations of those clouds in various regions for climate models. This factor can also be a useful tool for a simplified understanding of different roles of ice processes when mixed-phase clouds are compared to their warm-cloud counterparts in terms of the cloud development and its interactions with aerosols among those different systems. It should be noted that warm clouds have been studied much more than mixed-phase clouds, although mixed-phase clouds play as important roles as warm clouds in the evolution of climate and its change. This study provides preliminary mechanisms which differentiate mixed-phase clouds and their interactions with aerosols from their warm-cloud counterparts, and control the variation of the differentiation in different regions as a way of improving our understanding of mixed-phase clouds. It should be mentioned that the efficient way of developing general parameterizations, which are for climate models and consider all of warm, mixed-phase clouds in various regions and their interactions with aerosols, can be achieved by just adding those mechanisms to pre-existing parameterizations of much-studied warm clouds instead of developing brand new parameterizations from the scratch.

This study finds that the relation between ICNC/CDNC and IWC/LWC is highly non-linear. This high non-linearity is closely linked to how the number concentrations of CCN and INP, and associated ICNC/CDNC change. For a specific situation where the ICNC/CDNC variation is relatively small and both the number concentrations of CCN and INP reduce, the increase in ICNC/CDNC can reduce IWC/LWC, although it is found that as a whole, the increase in ICNC/CDNC enhances IWC/LWC. Hence, mechanisms identified in this study, especially regarding the use of ICNC/CDNC as a simplified and useful tool to explain differences in IWC/LWC among different cloud systems, are not complete and entirely general. In addition, results in this study are from only two cases in two specific locations in the midlatitude and Arctic regions and the more generalization of these results in this study merits more case studies over more locations in those regions, for example, in terms of above-mentioned sedimentation intensity, different factors (e.g., environmental factors) other than ICNC/CDNC, different sources and advection of aerosols, the magnitude of the variation of ICNC/CDNC and the way number concentrations of CCN and INP vary. Hence, findings particularly about relations between ICNC/CDNC and IWC/LWC in this study should be considered preliminary ones that initiate future work to streamline the development of the general parameterizations.

Code/Data source and availability

Our private computer system stores the code/data which are private and used in this study. Upon approval from funding sources, the data will be opened to the public. Projects related to this paper have not been finished, thus, the sources prevent the data from being open to the public currently. However, if information on the data is needed, contact the corresponding author Seoung Soo Lee (slee1247@umd.edu).

Author contributions

Essential initiative ideas are provided by SSL, CHJ and YJY to start this work. Simulation and observation data are analyzed by SSL, CHJ and JU. YZ, JP, MGM and SKS review the results and contribute to their improvement. JC provides supports to set up and run additional simulations during the review.

Competing interests

The authors declare that they have no conflict of interest.

Acknowledgements

This study is supported by the National Research Foundation of Korea (NRF) grant funded by the Korea government (MSIT) (Nos. NRF2020R1A2C1003215, NRF2020R1A2C2011081, NRF2023R1A2C1002367, NRF2021M1A5A1065672/KOPRI-PN23011 and 2020R1A2C1013278), and Basic Science Research Program through the NRF funded by the Ministry of Education (No. 2020R1A6A1A03044834).

References

Ackerman, A., Kirkpatrick, M., Stevens, D., et al.: The impact of humidity above stratiform clouds on indirect aerosol climate forcing, Science, 432, 1014–1017, https://doi.org/10.1038/nature03174, 2004.

Albrecht, B. A.: Aerosols, cloud microphysics, and fractional cloudiness, Science, 245, 1227-1230, 1989.

Bartosiewicz, Y., and Duponcheel, M.: Large eddy simulation: Application to liquid metal fluid flow and heat transfer . In: Roelofs, Ferry, Thermal Hydraulics Aspects of Liquid Metal Cooled Nuclear Reactors, Woodhead Publishing, 2018.

Brown, A., Milton, S., Cullen, M., Golding, B., Mitchell, J., and Shelly, A.: Unified modeling and prediction of weather and climate: A 25-year journey, B. Am. Meteorol. Soc., 93, 1865–1877, 2012.

Chen, F., and Dudhia, J.: Coupling an advanced land-surface hydrology model with the Penn State-NCAR MM5 modeling system. Part I: Model description and implementation, Mon. Wea. Rev., 129, 569–585, 2001.

Choi, Y.-S., Ho, C.-H., Park, C.-E., Storelvmo, T., and Tan, I.: Influence of cloud phase composition on climate feedbacks, J. Geophys. Res., 119, 3687–3700, doi:10.1002/2013JD020582, 2014.

Choi, Y.-S., Lindzen, R. S., Ho, C.-H., and Kim, J.: Space observations of cold-cloud phase change, Proc. Natl. Acad. Sci. U.S.A., 107, 11211–11216, 2010

Chua, X. R., and Ming, Y.: Convective invigoration traced to warm-rain microphysics, Geophys. Res. Lett, 47, https://doi.org/10.1029/2020GL089134, 2020.

Dione, C., Lohou, F., Lothon, M., Adler, B., Babić, K., Kalthoff, N., Pedruzo-Bagazgoitia, X., Bezombes, Y., and Gabella, O.: Low-level stratiform clouds and dynamical features observed within the southern West African monsoon, Atmos. Chem. Phys., 19, 8979–8997, https://doi.org/10.5194/acp-19-8979-2019, 2019.

Donovan, D. P.: Ice-cloud effective particle size parameterization based on combined lidar, radar reflectivity, and mean Doppler velocity measurements, J. Geophys. Res., 108, 4573, doi:10.1029/2003JD003469, 2003.

Donovan, D. P., and van Lammeren, A. C. A. P.: Cloud effective particle size and water content profile retrievals using combined lidar and radar observations: 1. Theory and examples, J. Geophys. Res., 106, 27,425–27,448, 2001.

Donovan, D. P., van Lammeren, A.C.A.P. , Hogan, R. J., Russchenberg, H. W. J., Apituley, A., Francis, P., Testud, J., Pelon, J., Quante, M., and Goddard, J. W. F.: Cloud effective particle size and water content profile retrievals using combined lidar and radar observations – 2. Comparison with IR radiometer and in situ measurements of ice clouds, J. Geophys. Res, 106, 27449-27464, 2001.

Dudhia, J.: Nemerical study of convection observed during the winter monsoon Experiment using a mesoscale two-dimensional Model, J. Atmos. Sci., 46, 3077–3107, https://doi.org/10.1175/1520-0469, 1989.

Fan, J., Rosenfeld, D., Zhang, Y., Giangrande, S. E., Li, Z., Machado, L. A. T., Martin, S. T., Yang, Y., Wang, J., and Artaxo, P.: Substantial convection and precipitation enhancements by ultrafine aerosol particles. Science, 359, 411–418, 2018

Forster, P., et al., Changes in atmospheric constituents and in radiative forcing, in: Climate change 2007: the physical science basis, Contribution of working group I to the Fourth Assessment Report of the Intergovernmental Panel on Climate Change, edited by Solomon, S., et al., Cambridge Univ. Press, New York, 2007.

Gettelman, A., Liu, X., Barahona, D., et al.: Climate impacts of ice nucleation, J. Geophys. Res., 117, D20201, doi:10.1029/2012JD017950, 2012.

Gras, J. L.: Southern hemisphere tropospheric aerosol microphysics, J. Geophys. Res., 96, 5345-5356.

Hahn, C. J., and Warren, S. G.: A gridded climatology of clouds over land (1971–96) and ocean (1954–97) from surface observations worldwide, Numeric Data Package NDP-026EORNL/CDIAC-153, CDIAC, Department of Energy, Oak Ridge, TN, 2007.

Hannak, L., Knippertz, P., Fink, A. H., Kniffka, A., and Pante, G.: Why do global climate models struggle to represent low-level clouds in the West African summer monsoon?, J. Climate, 30, 1665–1687, https://doi.org/10.1175/JCLI-D-16-0451.1, 2017

Hartmann, D. L., Ockert-Bell, M. E., and Michelsen, M. L.: The effect of cloud type on earth's energy balance—Global analysis, J. Climate, 5, 1281–1304, 1992.

Hartmann, M., Gong, X., Kecorius, S., van Pinxteren, M., Vogl, T., Welti, A., Wex, H., Zeppenfeld, S., Herrmann, H., Wiedensohler, A., and Stratmann, F.: Terrestrial or marine – indications towards the origin of ice-nucleating particles during melt season in the European Arctic up to 83.7° N, Atmos. Chem. Phys., 21, 11613–11636, https://doi.org/10.5194/acp-21-11613-2021, 2021.

Hogan, R. J., Illingworth, A. J., O'Connor, E. J., et al.: Cloudnet: Evaluation of model clouds using ground-based observations, ECMWF Workshop on parametrization of clouds on large-scale models., 2006.

IPCC: Climate Change: The Physical Science Basis. Contribution of Working Group I to the Sixth Assessment Report of the Intergovernmental Panel on Climate Change [Masson-Delmotte, V., Zhai, P., Pirani, A., Connors, S. L., Péan, C., Berger, S., Caud, N., Chen, Y., Goldfarb, L., Gomis, M. I., Huang, M., Leitzell, K., Lonnoy, E., Matthews, J. B. R., Maycock, T. K., Waterfield, T., Yelekçi, O., Yu, R., and Zhou, B. (eds.)]. Cambridge University Press, Cambridge, United Kingdom and New York, NY, USA, In press, doi:10.1017/9781009157896, 2021.

Jaenicke, R.: Tropospheric aerosols in Aerosol-Cloud-Climate Interactions, Hobbs, P. V., ed., Academic Press, San Diego, CA, pp. 1-31.

Jiang, H., Feingold, G. and Cotton, W. R: Simulations of aerosol-cloud-dynamical feedbacks resulting from entrainment of aerosol into the marine boundary layer during the Atlantic Stratocumulus Transition Experiment, J. Geophys. Res., 107(D24), 4813, doi:10.1029/2001JD001502, 2002.

Jung, C. H., Yoon, Y. J., Kang, H. J., Gim, Y., Lee, B. Y., Ström, J., Krejci, R., and Tunved, P.: The seasonal characteristics of cloud condensation nuclei (CCN) in the arctic lower troposphere, Tellus B: Chemical and Physical Meteorology, 70:1, 1513291, https://doi: 10.1080/16000889.2018.1513291, 2018.

Khain, A. P., Ovchinnikov, M., Pinsky, M., Pokrovsky, A. and Krugliak, H.: Notes on the state-of-the-art numerical modeling of cloud microphysics, Atmos. Res., 55, 159–224, 2000.

Khain, A., Pokrovsky, A., Rosenfeld, D., Blahak, U., and Ryzhkoy, A.: The role of CCN in precipitation and hail in a mid-latitude storm as seen in simulations using a spectral (bin) microphysics model in a 2D dynamic frame, Atmos. Res., 99, 129–146, 2011.

Khain, A. P., Phillips, V., Benmoshe, N., Pokrovsky, A.: The role of small soluble aerosols in the microphysics of deep maritime clouds, J. Atmos. Sci., 69, 2787–2807, 2012.

Knippertz, P., Fink, A. H., Schuster, R., Trentmann, J., Schrage, J. M., and Yorke, C.: Ultra-low clouds over the southern West African monsoon region, Geophys. Res. Lett., 38, L21808, https://doi.org/10.1029/2011GL049278, 2011.

Kogan, Y., 2013: A cumulus cloud microphysics parameterization for cloud-resolving models, J. Atmos. Sci., 70, 1423–1436, https://doi:10.1175/JAS-D-12-0183.1, 2013.

Koop, T., Luo, B. P., Tsias, A., and Peter, T.: Water activity as the determinant for homogeneous ice nucleation in aqueous solutions, Nature, 406, 611-614.

Lee, H., and Baik, J.-J.: A physically based autoconversion parameterization, J. Atmos. Sci., 74, 1599-1616, https://doi.org/10.1175/JAS-D-16-0207.1, 2017.

Lee S. S., Penner, J. E., and Saleeby, S. M.: Aerosol effects on liquid-water path of thin stratocumulus clouds, J. Geophys. Res., 114, D07204, doi:10.1029/2008JD010513, 2009.

Lee, S. S., et al., Mid-latitude mixed-phase stratocumulus clouds and their interactions with aerosols: how ice processes affect microphysical, dynamic and thermodynamic development in those clouds and interactions?, Atmos. Chem. Phys., https://doi.org/10.5194/acp-21-16843-2021, 2021.

Li, J., Carlson, B. E., Yung, Y. L., Lv, D., Hansen, J., Penner, J. E., Liao, H., Ramaswamy, V., Kahn, R. A., Zhang, P., Dubovik, O., Ding, A., Lacis, A. A., Zhang, L., and Dong, Y.: Scattering and absorbing aerosols in the climate system, Nature Reviews Earth and Environment, 3, 363–379, https://doi.org/10.1038/s43017-022-00296-7, 2022.

Lilly, D. K.: The representation of small scale turbulence in numerical simulation experiments, Proc. Ibm Sci. Comput. Symp. Environ. Sci., 320–1951, 195–210, 1967.

Lim, K.-S. S., and Hong, S.-Y.: Development of an effective double-moment cloud microphysics scheme with prognostic cloud condensation nuclei (CCN) for weather and climate models, Mon. Wea. Rev., 138, 1587–1612, doi:10.1175/2009MWR2968.1., 2010.

Liu, Y., and Daum, P. H.: Parameterization of the autoconversion. Part I: Analytical formulation of the Kessler-type parameterizations, J. Atmos. Sci., 61, 1539–1548, doi:10.1175/1520-0469(2004)061,1539:POTAPI.2.0.CO;2, 2004.

Lohmann, U., and Diehl, K.: Sensitivity studies of the importance of dust ice nuclei for theindirect aerosol effect on stratiform mixed-phase clouds, J. Atmos. Sci., 63, 968-

982, 2006.

Mansell, E. R., Ziegler, C. L., and Bruning, E. C., Simulated electrification of a small thunderstorm with two-moment bulk microphysics, J. Atmos. Sci., 67, 171–194, doi:10.1175/2009JAS2965.1., 2010.

Ming, Y., and Chua, X. R.: Convective invigoration traced to warm-rain microphysics, Geophys. Res. Lett., 47, doi.org/10.1029/2020GL089134, 2020.

Mlawer, E. J., Taubman, S. J., Brown, P. D., Iacono, M. J., and Clough, S. A.: RRTM, a validated correlated-k model for the longwave, J. Geophys. Res., 102, 16663-1668, 1997.

Moeng, C.-H., Sullivan, P. P., and Stevens, B.: Including radiative effects in an entrainment rate formula for buoyancy-driven PBLs, J. Atmos. Sci., 56, 1031 – 1049, doi:10.1175/1520-0469(1999)056<1031:IREIAE>2.0.CO;2, 1999.

Möhler, O., et al, Efficiency of the deposition mode ice nucleation on mineral dustparticles, Atmos. Chem. Phys., 6, 3007-3021, 2006.

Morrison, H., deBoer, G., Feingold, G., Harrington, J., Shupe, M., and Sulia, K., Resilience of persistent Arctic mixed-phase clouds, Nat. Geosci., 5, 11–17, https://doi.org/10.1038/ngeo1332, 2012.

Morrison, H., Curry, J. A., and Khvorostyanov, V. I., A new double-moment microphysics parameterization for application in cloud and climate models. Part I: Description, J. Atmos. Sci., 62, 1665–1677, 2005.

Morrison, H., hompson, G., and V. Tatarskii, Impact of cloud microphysics on the development of trailing stratiform precipitation in a simulated squall line: Comparison of one- and two-moment schemes. Mon. Wea. Rev., 137, 991–1007, https://doi.org/10.1175/2008MWR2556.1., 2009.

Murakami, M., 1990, Numerical modeling of the dynamical and microphysical evolution of an isolated convective cloud—The July 19 1981 CCOPE cloud, J. Meteor. Soc. Japan, 68, 107–128.

Ovchinnikov, M., Korolev, A., and Fan, J.: Effects of ice number concentration on dynamics of a shallow mixed-phase stratiform cloud, J. Geophys. Res., 116, D00T06, doi:10.1029/2011JD015888, 2011.

Possner, A., Ekman, A. M. L., and Lohmann, U.: Cloud response and feedback processes in stratiform mixed-phase clouds perturbed by ship exhaust, Geophys. Res. Lett., 44, 1964–1972, https://doi.org/10.1002/2016GL071358, 2017.

Pruppacher, H. R. and Klett, J. D.: Microphysics of clouds and precipitation, 714pp, D. Reidel, 1978.

Ramaswamy, V., et al.: Radiative forcing of climate change, in Climate Change 2001: The Scientific Basis, edited by J. T. Houghton et al., 349-416, Cambridge Univ. Press, New York, 2001.

Seinfeld, J. H., and Pandis, S. N.: Atmospheric chemistry and physics: From air pollution to climate change, John Wiley & Sons, 1326 pp, 1998.

Solomon, A., de Boer, G., Creamean, J. M., McComiskey, A., Shupe, M. D., Maahn, M., and Cox, C.: The relative impact of cloud condensation nuclei and ice nucleating particle concentrations on phase partitioning in Arctic mixed-phase stratocumulus clouds, Atmos. Chem. Phys., 18, 17047–17059, https://doi.org/10.5194/acp-18-17047-2018, 2018.

Smagorinsky, J.: General circulation experiments with the primitive equations, Mon. Wea. Rev., 91, 99–164, 1963.

Stevens, B., et al.: On entrainment rates in nocturnal marine stratocumulus, Q. J. R. Meteorol. Soc., 129, 3469 – 3492, doi:10.1256/qj.02.202, 2003a.

Stevens, B., et al.: Dynamics and chemistry of marine stratocumulus-DYCOMS-II, Bull. Am. Meteorol. Soc., 84, 579– 593, doi:10.1175/BAMS-84-5-579, 2003b.

Stevens, B., and Feingold, G.: Untangling aerosol effects on clouds and precipitation in a buffered system, Nature, 461, 607–613, https://doi.org/10.1038/nature08281, 2009.

Stephens, G. L., and Greenwald, T. J.: Observations of the Earth's radiation budget in relation to atmospheric hydrology. Part II: Cloud effects and cloud feedback, J. Geophys. Res., 96, 15 325–15 340, 1991.

Tinel, C., Testud, J., Hogan, R. J., Protat, A., Delanoe, J. and Bouniol, D.: The retrieval of ice cloud properties from cloud radar and lidar synergy, J. Appl. Meteorol., 44, 860-875, 2005.

Tsushima, Y., Webb, M. J., Williams, K. D., Soden, B. J., et al.: Importance of the mixed-phase cloud distribution in the control climate for assessing the response of clouds to carbon dioxide increase: A multi-model study, Clim. Dyn., 27, 113–126, 2006.

Tunved, P., Ström, J. and Krejci, R.: Arctic aerosol life cycle: linking aerosol size distributions observed between 2000 and 2010 with air mass transport and precipitation at Zeppelin station, Ny-Ålesund, Svalbard, Atmos. Chem. Phys., 13, 3643–3660, https://doi:10.5194/acp-13-3643-2013, 2013

Twomey, S.: Pollution and the Planetary Albedo, Atmos. Env., 8,1251-1256, 1974.

Warren, S. G., Hahn, C. J., London, J., Chervin, R. M., and Jenne, R. L.: Global distribution of total cloud cover and cloud types over land, NCAR Tech. Note NCAR/TN-273+STR, National Center for Atmospheric Research, Boulder, CO, 29 pp. + 200 maps, 1986.

Wood, R.: Stratocumulus clouds, Mon. Wea. Rev., 140, 2373-2423, 2012.

Xue, L., Teller, A., Rasmussen, R. M., Geresdi, I., and Pan, Z.: Effects of aerosol solubility and regeneration on warm-phase orographic clouds and precipitation simulated by a detailed bin microphysical scheme, J. Atmos. Sci., 67, 3336–3354, 2010.

Zhang, D., Vogelmann, A., Kollias, P., Luke, E., Yang, F., Lubin, D., and Wang, Z.: Comparison of Antarctic and Arctic single-layer stratiform mixed-phase cloud properties using ground-based remote sensing measurements, J. Geophys. Res., 124, 10186–10204, https://doi.org/10.1029/2019JD030673, 2019.

Zheng, Y., Zhang, H., Rosenfeld, D., Lee, S. S., Su, T., and Li, Z.: Idealized Large-Eddy Simulations of Stratocumulus Advecting over Cold Water. Part I: Boundary Layer Decoupling, 78, 4089-4102, https://doi.org/10.1175/JAS-D-21-0108.1, 2021.

FIGURE CAPTIONS

Figure 1. A red rectangle marks the simulation domain in the Svalbard area, Norway. The light blue represents the ocean and the green the land area.

Figure 2. (a) The vertical distributions of the domain-averaged potential temperature and humidity at the first time step, (b) the time series of the domain-averaged large-scale subsidence or downdraft at the model top and (c) the time series of the domain-averaged surface temperature.

Figure 3. Aerosol size distribution at the surface. N represents aerosol number concentration per unit volume of air and D represents aerosol diameter.

Figure 4. The vertical distributions of the time- and domain-averaged IWC and LWC in the 200_2 and 200_0 runs.

Figure 5. The time series of (a) observed and simulated cloud-top and bottom heights, (b) retrieved and simulated IWP, and observed and simulated LWP, and (c) the simulated surface sensible and latent heat fluxes. For the time series, the simulated cloud-top height is averaged over grid points with cloud tops and the simulated cloud-bottom height is averaged over grid points with cloud bottoms, while the simulated IWP and LWP are averaged over grid points with non-zero IWP and LWP, respectively, at each time step in the 200_2 run. The simulated surface sensible and latent heat fluxes are averaged over the horizontal domain at the surface and each time step in the 200_2 run.

Figure 6. The vertical distributions of the time- and domain-averaged deposition and condensation rates in the 200_2 and 200_0 runs.

Figure 7. The time series of the average supersaturation with respect to ice and water over grid points where deposition occurs in the presence of both droplets and ice crystals in the 200_2 run.

Figure 8. The vertical distributions of the time- and domain-averaged IWC and LWC in the 200_2, 200_0 and 200_0.07 runs.

Figure 9. The vertical distributions of the time- and domain-averaged (a) IWC in the 200_2, 2000_20, 200_0.07, 200_20, 2000_2, 2000_0.07, and 200_0.7 runs. (b) The vertical distributions of the time- and domain-averaged LWC in the 200_0 and 2000_0 runs as well as all the runs shown in panel (a).

Figure 10. The average size distributions of (a) ice crystals over grid points with non-zero IWC and the simulation period and (b) drops over grid points with non-zero LWC and the simulation period.

Simulations	The number concentration of aerosols acting as CCN at the first time step in the PBL (cm^{-3})	The number concentration of aerosols acting as INP at the first time step in the PBL (cm^{-3})	ICNCavg/CDNCavg	Ice processes	Radiation
200_2	200	2	0.220	Present	Present
2000_20	2000	20	0.201	Present	Present
2000_2	2000	2	0.108	Present	Present
200_20	200	20	0.512	Present	Present
200_0	200	2	0.000	Absent	Present
2000_0	2000	2	0.000	Absent	Present
200_0.07	200	0.07	0.022	Present	Present
2000_0.07	2000	0.07	0.012	Present	Present
200_0.7	200	0.7	0.041	Present	Present
4000_45	4000	45	0.220	Present	Present
13_0.1	13	0.1	0.220	Present	Present
4000_1.8	4000	1.8	0.022	Present	Present
12_0.0035	12	0.0035	0.022	Present	Present

Table 1. Summary of simulations

Simulations	IWC (10^{-3} g m^{-3})	LWC (10^{-3} g m^{-3})	IWP (g m^{-2})	LWP (g m^{-2})	IWC/LWC	IWP/LWP	Condensation rate		Deposition rate		Cloud-base sedimentation (10^{-3} g m^{-2} s^{-1})		Entrainment (cm s^{-1})
							Over grid points (10^{-2} g m^{-3} s^{-1})	Over cloudy columns (g m^{-2} s^{-1})	Over grid points (10^{-2} g m^{-3} s^{-1})	Over cloudy columns (g m^{-2} s^{-1})	Ice-crystal	Droplet	
200_2	6.57	0.25	31.94	1.23	26.28	25.96	0.11	1.98	1.30	23.40	1.17	0.17	0.25
2000_20	7.82	0.21	40.91	1.08	37.24	37.91	0.09	1.62	1.57	28.26	0.94	0.06	0.53
2000_2	6.55	0.29	31.85	1.46	22.58	21.81	0.12	2.16	1.28	23.04	1.11	0.08	0.28
200_20	7.80	0.20	40.82	1.01	39.00	40.42	0.09	1.62	1.56	28.08	0.97	0.11	0.51
200_0	0.00	2.06	0.00	10.35	0.00	0.00	0.72	12.48	0.00	0.00	0.00	0.36	0.08
2000_0	0.00	2.25	0.00	11.29	0.00	0.00	0.76	12.80	0.00	0.00	0.00	0.14	0.10
200_0.07	0.89	0.85	4.27	4.20	1.05	1.02	0.32	5.76	0.35	6.30	0.19	0.28	0.06
2000_0.07	0.79	0.97	3.82	4.83	0.81	0.79	0.38	6.84	0.31	5.58	0.17	0.19	0.07
200_0.7	0.98	0.78	4.73	3.88	1.25	1.22	0.31	5.58	0.39	7.02	0.14	0.22	0.07

Table 2. The averaged IWC, LWC, IWP, LWP, condensation and deposition rates over all of grid points and the simulation period in each of simulations. IWC/LWC (IWP/LWP) is the averaged IWC (IWP) over the averaged LWC (LWP). Also, as shown are the vertically integrated condensation and deposition rates over each cloudy column which are averaged over those columns and the simulation period. The average cloud-base sedimentation rate, which is for each of ice crystals and droplets, over the cloud base and simulation period, and the average cloud-top entrainment rate over the cloud top and simulation period are shown as well.

Simulations	IWC (10^{-3} g m^{-3})	LWC (10^{-3} g m^{-3})	IWP (g m^{-2})	LWP (g m^{-2})	IWC/LWC	IWP/LWP	Condensation rate		Deposition rate		Cloud-base sedimentation (10^{-3} g m^{-2} s^{-1})		Entrainment (cm s^{-1})
							Over grid points (10^{-2} g m^{-3} s^{-1})	Over cloudy columns (g m^{-2} s^{-1})	Over grid points (10^{-2} g m^{-3} s^{-1})	Over cloudy columns (g m^{-2} s^{-1})	Ice-crystal	Droplet	
200_2_norad	6.42	0.24	31.21	1.22	26.75	25.58	0.10	1.96	1.29	23.35	1.16	0.16	0.24
2000_20_norad	7.63	0.21	40.05	1.07	36.33	37.42	0.09	1.59	1.55	29.91	0.92	0.06	0.51
2000_2_norad	6.40	0.29	31.11	1.45	22.06	21.45	0.11	2.12	1.26	22.69	1.07	0.08	0.27
200_20_norad	7.61	0.20	39.95	0.99	38.05	40.35	0.09	1.59	1.54	27.72	0.97	0.11	0.49
200_0_norad	0.00	2.03	0.00	10.20	0.00	0.00	0.72	12.31	0.00	0.00	0.00	0.34	0.08
2000_0_norad	0.00	2.21	0.00	11.12	0.00	0.00	0.75	12.63	0.00	0.00	0.00	0.13	0.10
200_0.07_norad	0.87	0.84	4.21	4.17	1.04	1.01	0.31	5.74	0.35	6.21	0.18	0.27	0.05
2000_0.07_norad	0.78	0.96	3.78	4.80	0.81	0.79	0.36	6.81	0.30	5.50	0.16	0.18	0.06
200_0.7_norad	0.97	0.76	4.70	3.85	1.25	1.22	0.30	5.55	0.38	6.91	0.13	0.21	0.06

Table 3. Same as Table 2 but for the repeated simulations with radiative processes turned off.

Simulations	ICNCavg/CDNCavg	Percentage increases (+) or decrease (-) in ICNCavg/CDNCavg	IWC/LWC	Percentage increases (+) or decrease (-) in IWC/LWC
2000_0.07	0.012		0.81	
200_0.07	0.022	+83.33%	1.05	+29.6%
200_0.7	0.041	+86.36%	1.25	+19.0%
2000_2	0.108	+163.4%	22.58	+1706.4%
2000_20	0.201	+86.1%	37.24	+64.9%
200_2	0.220	+9.4%	26.28	-29.4%
200_20	0.512	+132.7%	39.00	+48.4%

Table 4. ICNCavg/CDNCavg and IWC/LWC in the simulations that are related to Section 4.1. The Percentage increases or decreases in ICNCavg/CDNCavg and IWC/LWC as shown in the ith row are $\frac{(\mathrm{ICNCavg/CDNCavg})_i - (\mathrm{ICNCavg/CDNCavg})_{i-1}}{(\mathrm{ICNCavg/CDNCavg})_{i-1}} \times 100\,(\%)$ and $\frac{(\mathrm{IWC/LWC})_i - (\mathrm{IWC/LWC})_{i-1}}{(\mathrm{IWC/LWC})_{i-1}} \times 100\,(\%)$, respectively. Here, $(\mathrm{ICNCavg/CDNCavg})_i$ and $(\mathrm{IWC/LWC})_i$ represent ICNCavg/CDNCavg and IWC/LWC in the ith row, respectively.

Simulations	ICNCavg/CDNCavg	IWC/LWC	Percentage increases (+) or decrease (-) in IWC/LWC
Polar case			
200_2	0.220	26.28	
4000_45	0.220	27.25	+3.7%
13_0.1	0.220	25.62	-2.5%
Representing midlatitude case			
200_0.07	0.022	1.05	
4000_1.8	0.022	1.09	+3.8%
12_0.0035	0.022	1.02	-2.9%

Table 5. ICNCavg/CDNCavg and IWC/LWC in the simulations that are related to Section 4.2. The percentage increases or decreases in IWC/LWC in the 4000_45 run or in the 13_0.1 run are $\frac{(\mathrm{IWC/LWC})_{4000\_45\ or\ 13\_0.1} - (\mathrm{IWC/LWC})_{200\_2}}{(\mathrm{IWC/LWC})_{200\_2}} \times 100\ (\%)$. Here, $(\mathrm{IWC/LWC})_{4000\_45\ \mathrm{or}\ 13\_01}$ represents IWC/LWC in the 4000_45 run or the 13_01 run, while $(\mathrm{IWC/LWC})_{200\_2}$ represents IWC/LWC in the 200_2 run. The percentage increases or decreases in IWC/LWC in the 4000_1.8 run or the 12_0.0035 run are $\frac{(\mathrm{IWC/LWC})_{4000\_1.8\_fac10\ or\ 12\_0.0035\_fac10} - (\mathrm{IWC/LWC})_{200\_2\_fac10}}{(\mathrm{IWC/LWC})_{200\_2\_fac10}} \times 100\ (\%)$. Here, $(\mathrm{IWC/LWC})_{4000\_1.8\ \mathrm{or}\ 12\_0.0035}$ represents IWC/LWC in the 4000_1.8 run or the 12_0.0035 run, while $(\mathrm{IWC/LWC})_{200\_0.07}$ represents IWC/LWC in the 200_0.07 run.

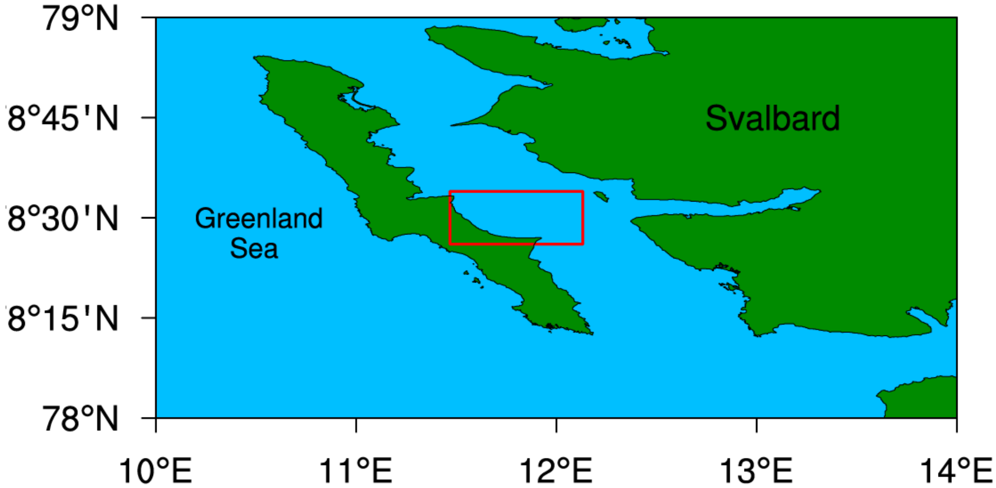
79°N
8°45'N
8°30'N
8°15'N
78°N
10°E
11°E
12°E
13°E
14°E
Svalbard
Greenland
Sea

Figure 1

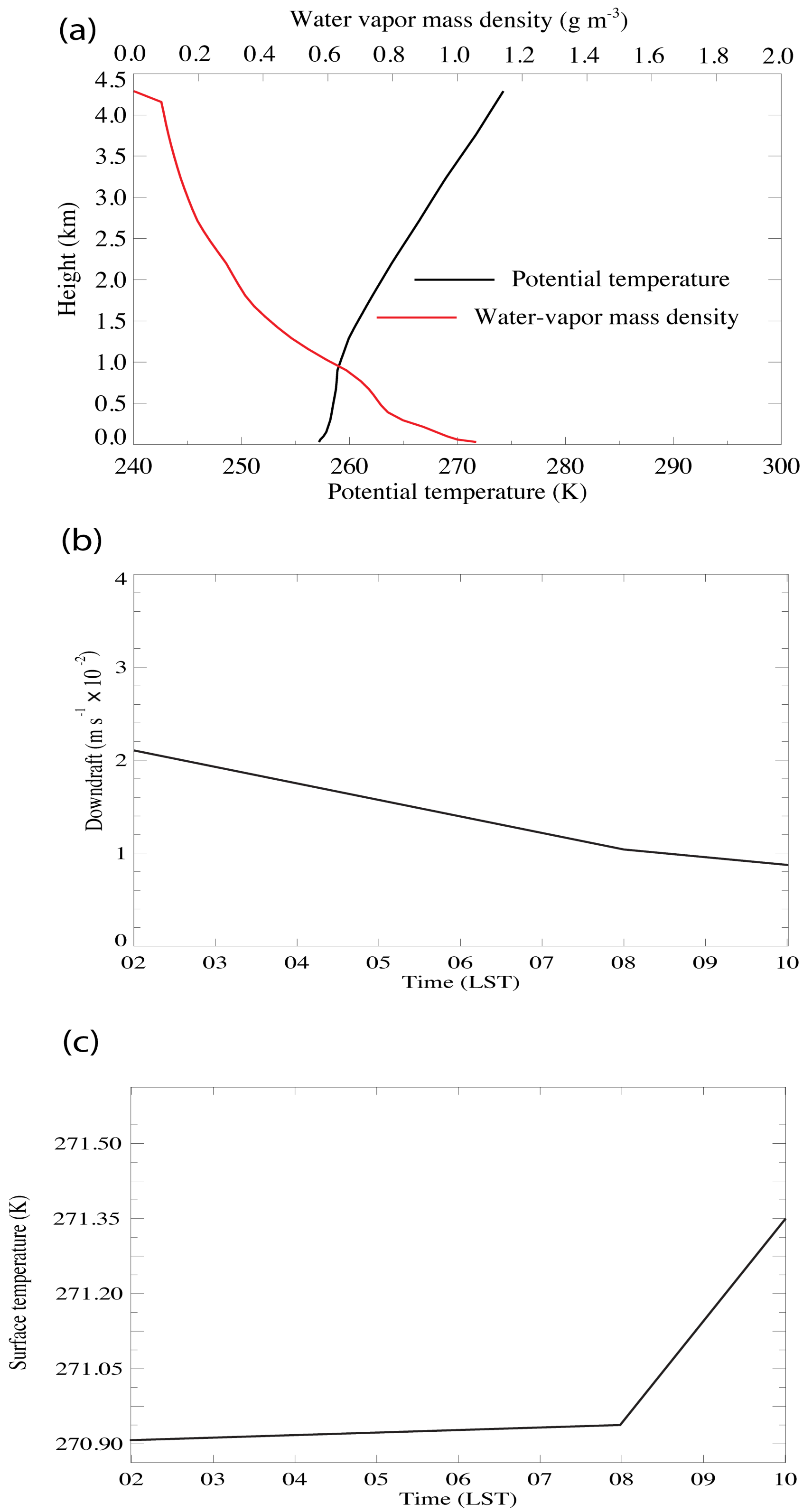
(a)
Water vapor mass density (g m-3)
0.0
0.2
0.4
0.6
0.8
1.0
1.2
1.4
1.6
1.8
2.0
Height (km)
4.5
4.0
3.5
3.0
2.5
2.0
1.5
1.0
0.5
0.0
Potential temperature
Water-vapor mass density
240
250
260
270
280
290
300
Potential temperature (K)
(b)
Downdraft (m s-1 x 10-2)
4
3
2
1
0
02
03
04
05
06
07
08
09
10
Time (LST)
(c)
Surface temperature (K)
271.50
271.35
271.20
271.05
270.90
02
03
04
05
06
07
08
09
10
Time (LST)

Figure 2

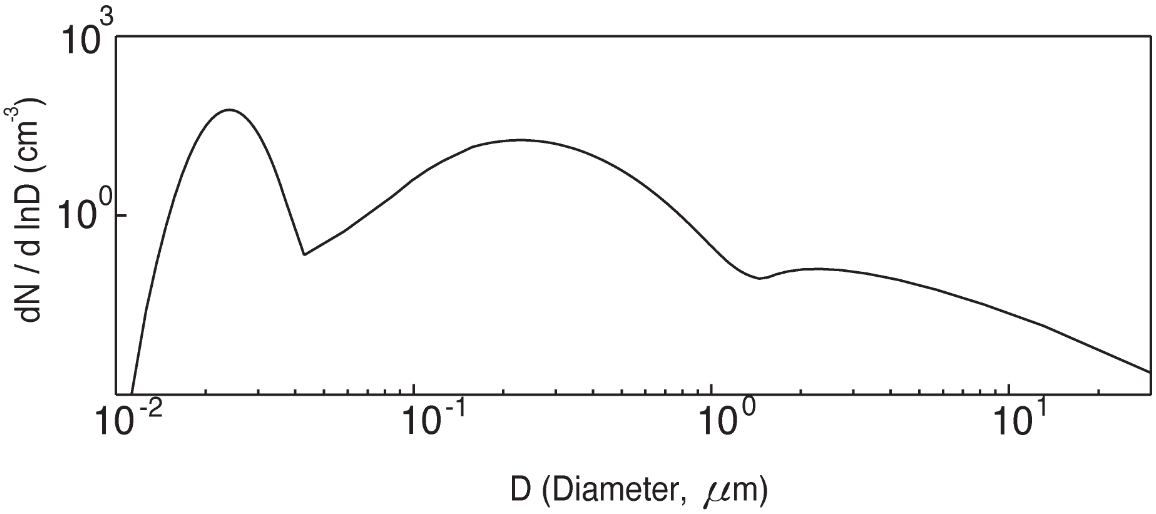

Figure 3

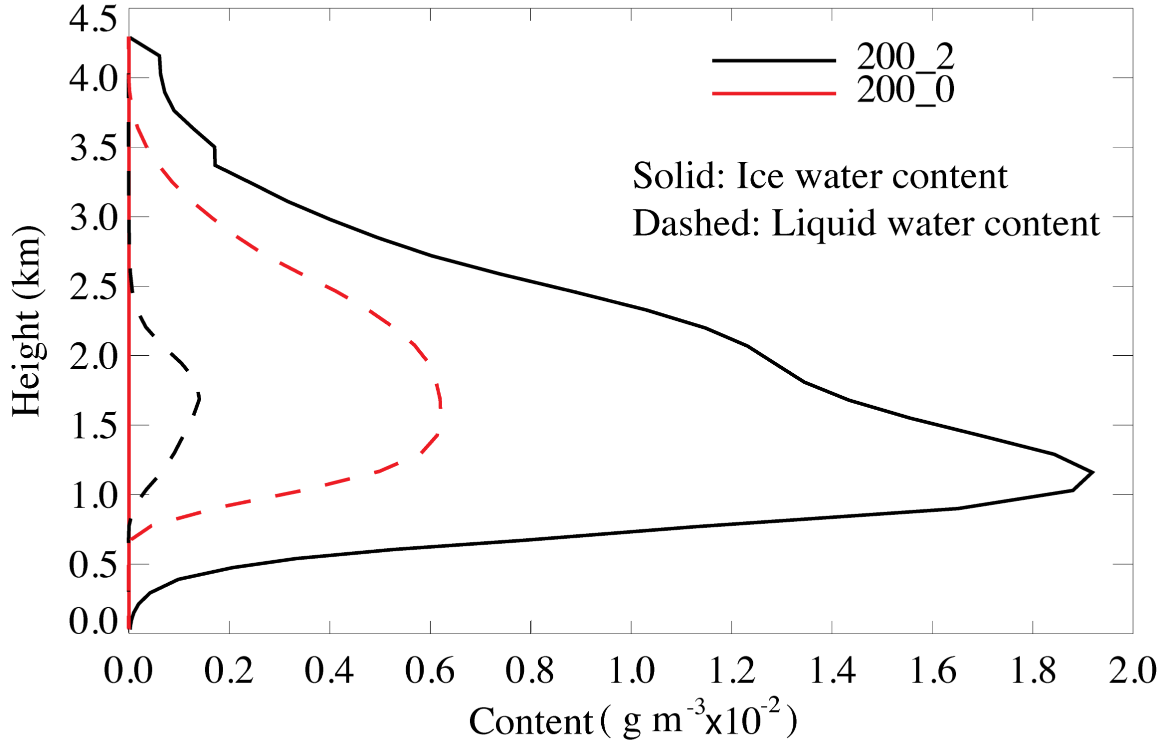
200_2
200_0
Solid: Ice water content
Dashed: Liquid water content
Height (km)
4.5
4.0
3.5
3.0
2.5
2.0
1.5
1.0
0.5
0.0
0.0 0.2 0.4 0.6 0.8 1.0 1.2 1.4 1.6 1.8 2.0
Content (g m^{-3}x10^{-2})

Figure 4

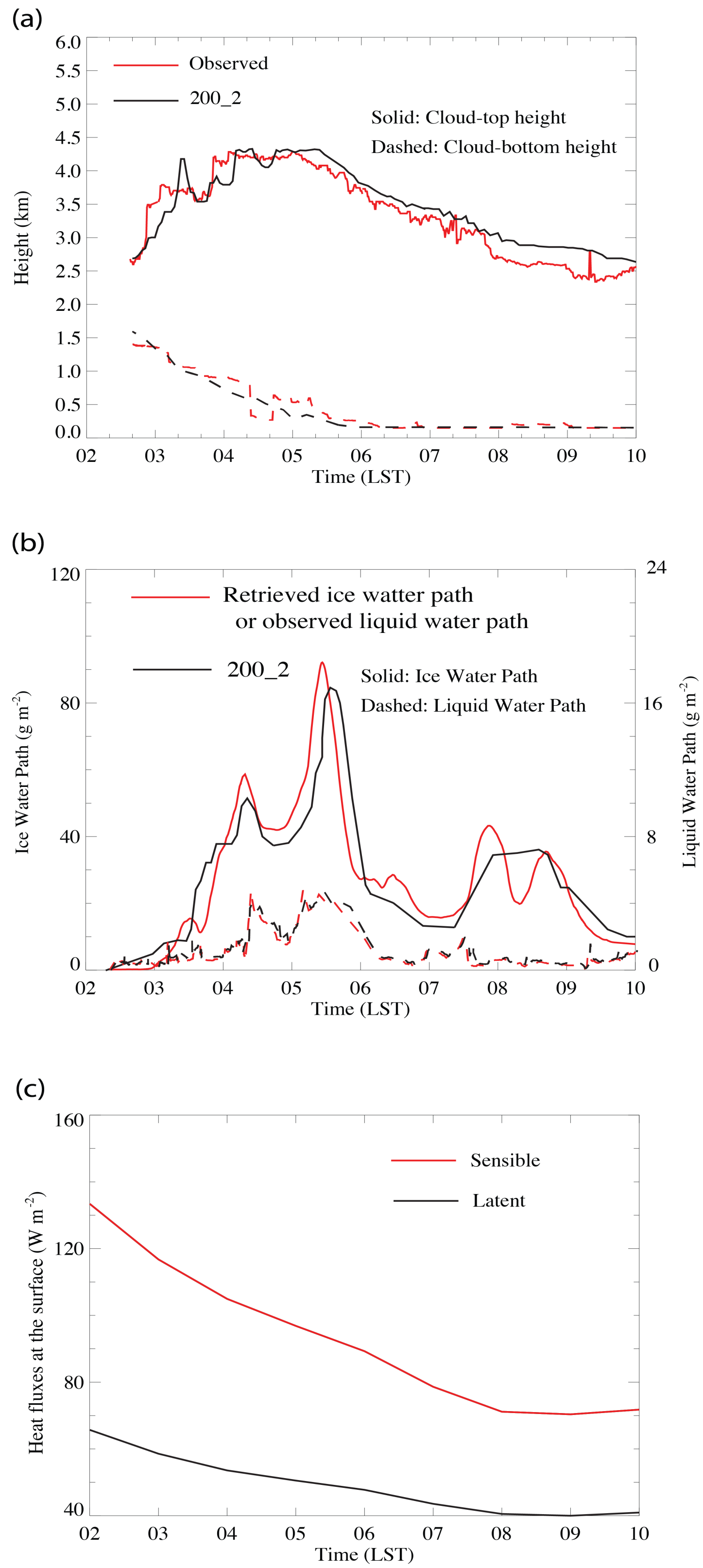
(a)
Observed
200_2
Solid: Cloud-top height
Dashed: Cloud-bottom height
Height (km)
6.0
5.5
5.0
4.5
4.0
3.5
3.0
2.5
2.0
1.5
1.0
0.5
0.0
02
03
04
05
06
07
08
09
10
Time (LST)
(b)
Retrieved ice watter path
or observed liquid water path
200_2
Solid: Ice Water Path
Dashed: Liquid Water Path
Ice Water Path (g m-2)
Liquid Water Path (g m-2)
120
80
40
0
24
16
8
0
02
03
04
05
06
07
08
09
10
Time (LST)
(c)
Sensible
Latent
Heat fluxes at the surface (W m-2)
160
120
80
40
02
03
04
05
06
07
08
09
10
Time (LST)

Figure 5

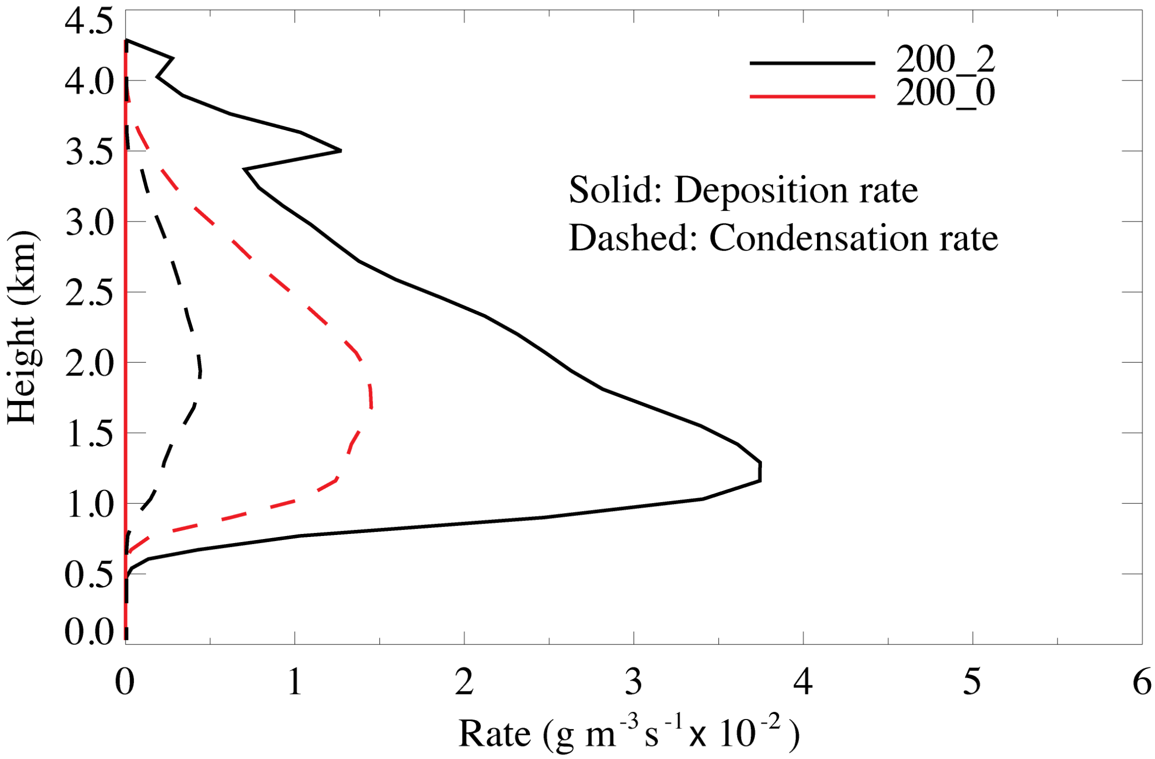
200_2
200_0
Solid: Deposition rate
Dashed: Condensation rate
Height (km)
Rate (g m-3 s-1 x 10-2)
4.5
4.0
3.5
3.0
2.5
2.0
1.5
1.0
0.5
0.0
0
1
2
3
4
5
6

Figure 6

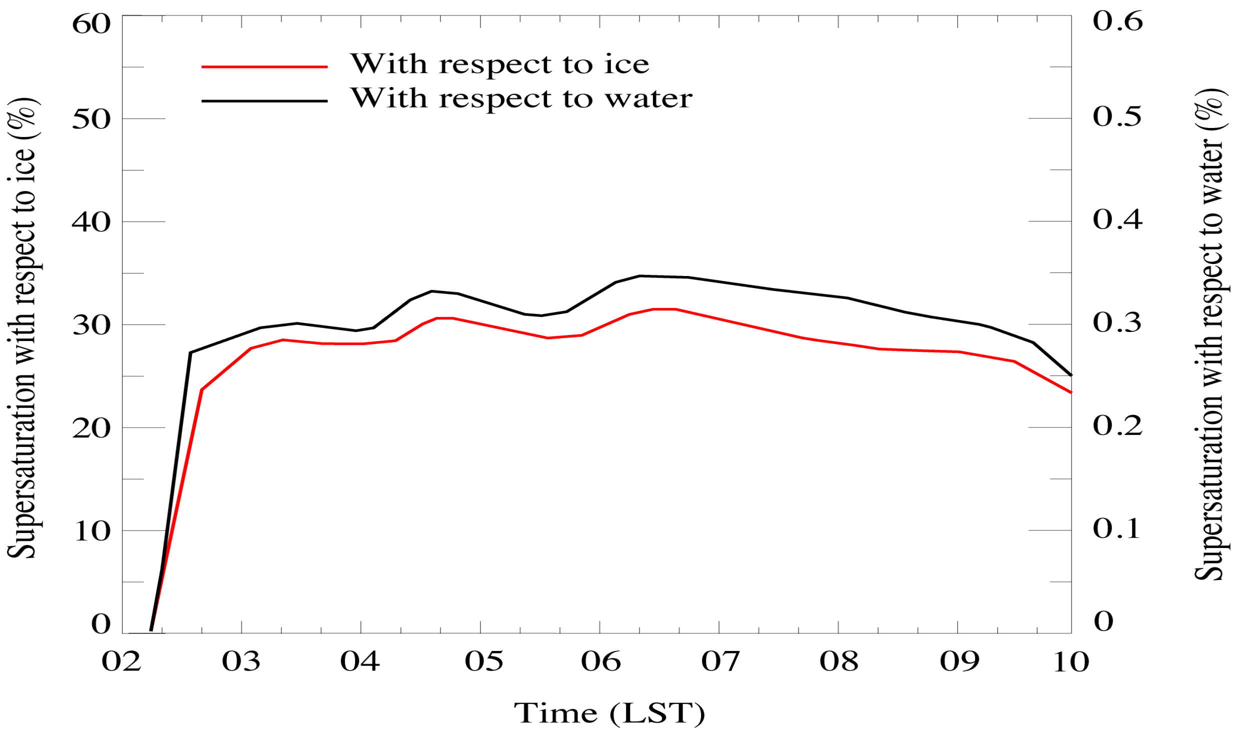
With respect to ice
With respect to water
Supersaturation with respect to ice (%)
Supersaturation with respect to water (%)
Time (LST)
0
10
20
30
40
50
60
0
0.1
0.2
0.3
0.4
0.5
0.6
02
03
04
05
06
07
08
09
10

Figure 7

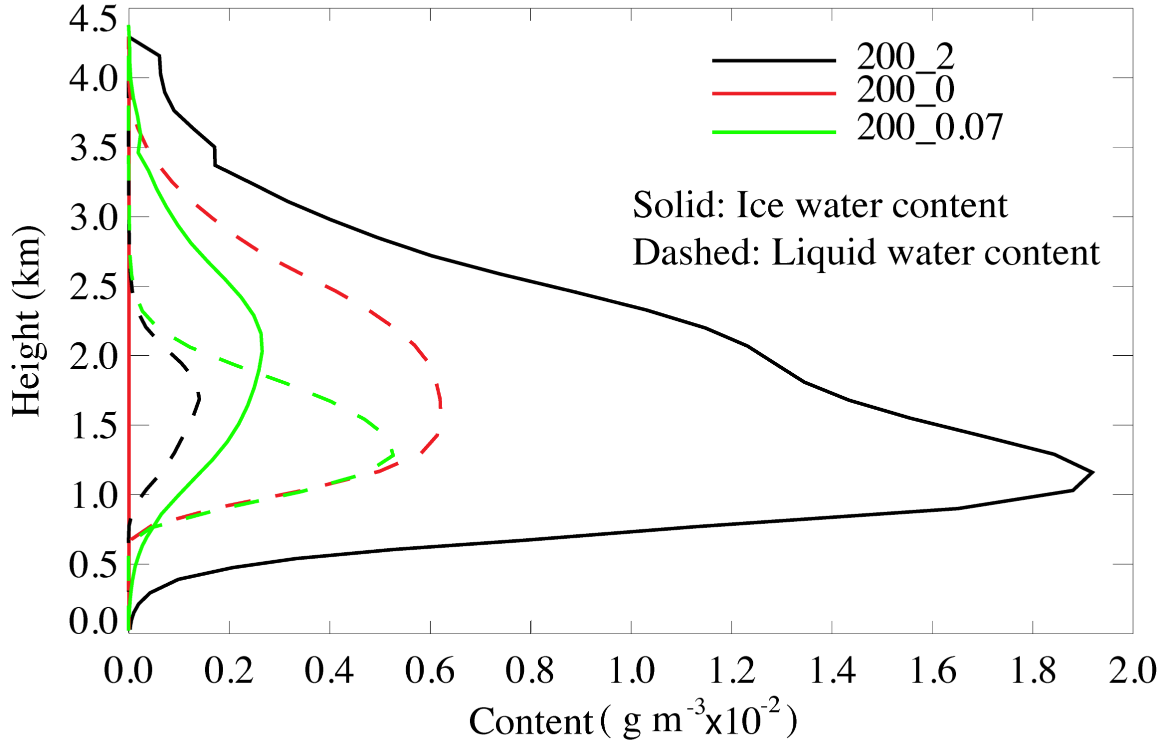
200_2
200_0
200_0.07
Solid: Ice water content
Dashed: Liquid water content
Height (km)
0.0
0.5
1.0
1.5
2.0
2.5
3.0
3.5
4.0
4.5
0.0
0.2
0.4
0.6
0.8
1.0
1.2
1.4
1.6
1.8
2.0
Content (g m-3x10-2)

Figure 8

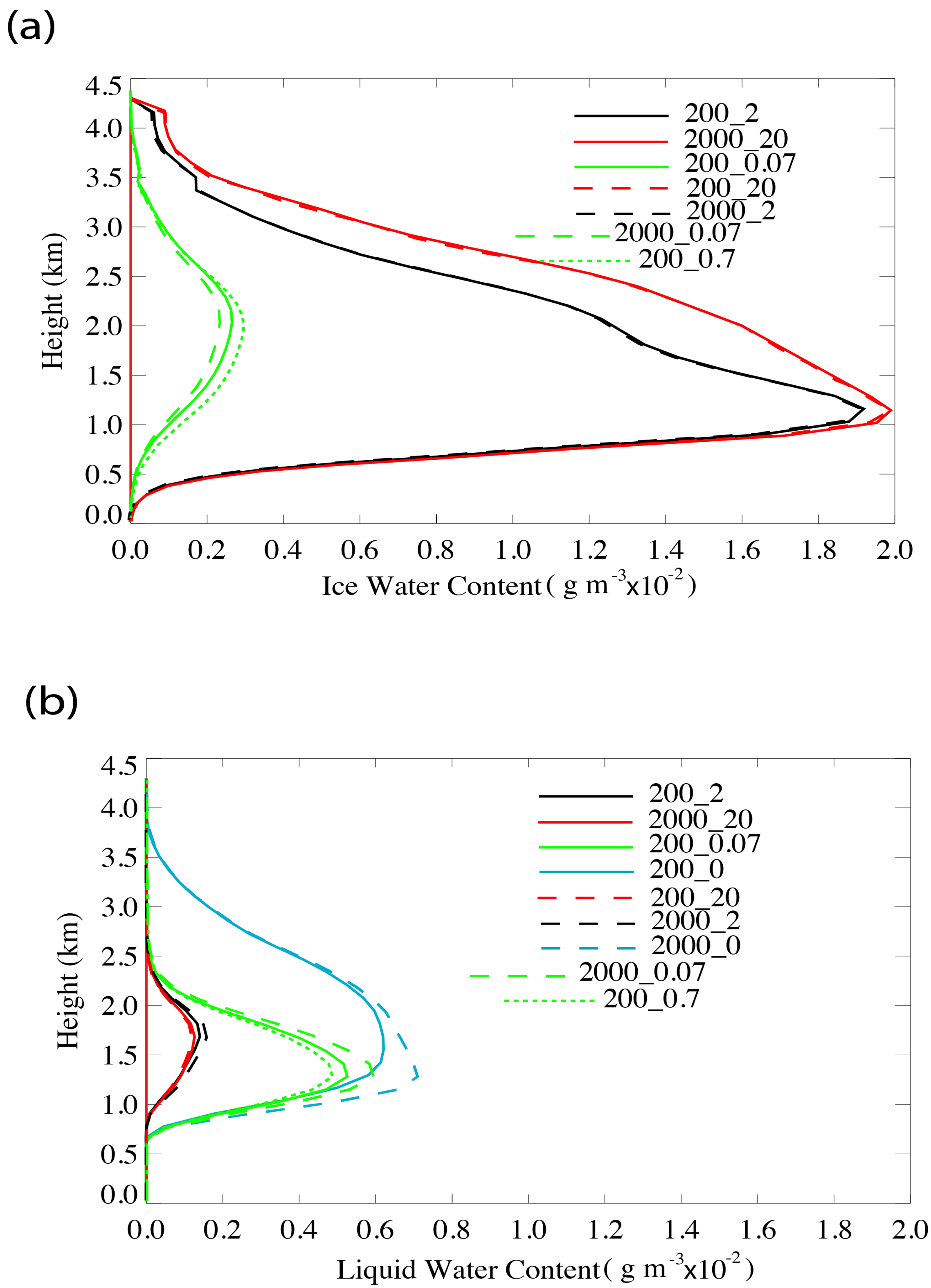

(a)
Height (km)
Ice Water Content (g m^{-3}x10^{-2})
200_2
2000_20
200_0.07
200_20
2000_2
2000_0.07
200_0.7
(b)
Height (km)
Liquid Water Content (g m^{-3}x10^{-2})
200_2
2000_20
200_0.07
200_0
200_20
2000_2
2000_0
2000_0.07
200_0.7

Figure 9

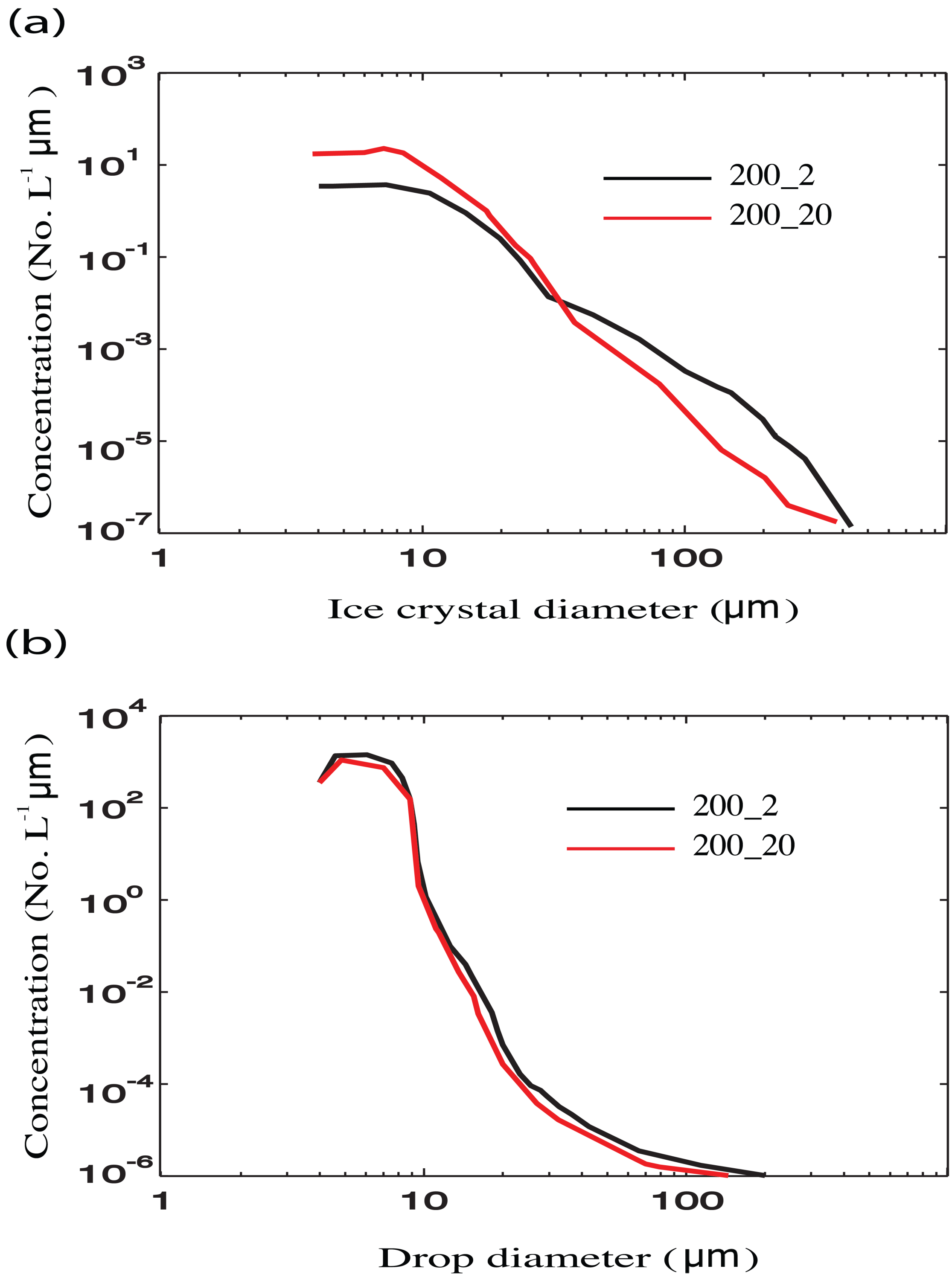
(a)
Concentration (No. L-1 µm)
10^3
10^1
10^-1
10^-3
10^-5
10^-7
1
10
100
Ice crystal diameter (µm)
200_2
200_20
(b)
Concentration (No. L-1 µm)
10^4
10^2
10^0
10^-2
10^-4
10^-6
1
10
100
Drop diameter (µm)
200_2
200_20

Figure 10